



The head anatomy of *Protanilla lini* (Hymenoptera: Formicidae: Leptanillinae), with a hypothesis of their mandibular movement

Adrian RICHTER, Francisco HITA GARCIA, Roberto A. KELLER, Johan BILLEN, Julian KATZKE, Brendon E. BOUDINOT, Evan P. ECONOMO & Rolf G. BEUTEL

Abstract

The hypogaecic ant subfamilies Leptanillinae and Martialinae likely form the sister group to the remainder of the extant Formicidae. In order to increase the knowledge of anatomy and functional morphology of these unusual and phylogenetically crucial ants, we document and describe in detail the cranium of a leptanilline, *Protanilla lini* TERAYAMA, 2009. The mandibular articulation of the species differs greatly from that of other ants studied so far, and clearly represents a derived condition. We propose a mode of movement for the specialized mandibles that involves variable rotation and sophisticated locking mechanisms. While a wide opening gape and a unique articulation are characteristics of the mandibular movement of *P. lini*, the observed condition differs from the trap-jaw mechanisms occurring in other groups of ants, and we cannot, at present, confirm such a functional configuration. *Protanilla lini* displays hardly any plesiomorphies relative to the ponerofornicine ants, with the possible exception of the absence of the torular apodeme. Instead, the species is characterized by a suite of apomorphic features related to its hypogaecic and specialized predatory lifestyle. This includes the loss of eyes and optic neuropils, a pronouncedly prognathous head, and the derived mandibular articulation. The present study is an additional stepping-stone on our way to reconstructing the cephalic ground plan of ants and will contribute to our understanding of ant evolution.

Key words: Animation, functional morphology, anatomy, skeletomusculature system, 3D reconstruction, μ -CT scan, trap-jaw ants.

Received 23 October 2020; revision received 7 January 2021; accepted 25 February 2021

Subject Editor: Flávia Esteves

Adrian Richter (contact author), Institut für Zoologie und Evolutionsforschung, FSU Jena, 07743 Jena, Germany; Biodiversity and Biocomplexity Unit, Okinawa Institute of Science and Technology Graduate University, Onna-son, Okinawa, 904-0495, Japan. E-mail: adrichter@gmx.de

Francisco Hita Garcia, Julian Katzke & Evan P. Economo, Biodiversity and Biocomplexity Unit, Okinawa Institute of Science and Technology Graduate University, Onna-son, Okinawa, 904-0495, Japan.

Roberto A. Keller, Biodiversity and Biocomplexity Unit, Okinawa Institute of Science and Technology Graduate University, Onna-son, Okinawa, 904-0495, Japan; MUHNAC / cE3c – Centre for Ecology, Evolution and Environmental Changes, Faculdade de Ciências da Universidade de Lisboa, 1749-016 Lisbon, Portugal.

Johan Billen, Zoological Institute, KU Leuven, 3000 Leuven, Belgium.

Brendon E. Boudinot, Institut für Zoologie und Evolutionsforschung, FSU Jena, 07743 Jena, Germany; Department of Entomology & Nematology, University of California, Davis, One Shields Ave, Davis, CA 95618.

Rolf G. Beutel, Institut für Zoologie und Evolutionsforschung, FSU Jena, 07743 Jena, Germany.

Introduction

The small subfamily Leptanillinae is potentially crucial for understanding the evolution of extant ants. Together with the cryptic species *Martialis heureka* RABELING & VERHAAGH, 2008 (Martialinae), they likely form a small monophyletic unit, Leptanillomorpha, which is probably the sister group of all remaining extant ants, referred to

as the ponerofornicine clade (BOROWIEC & al. 2019). The latter concept, that is, an early split of Leptanillinae, has been consistently confirmed in molecular phylogenetic studies (BRADY & al. 2006, MOREAU & al. 2006, BRANSTETTER & al. 2017, BOROWIEC & al. 2019), although with some uncertainty concerning the placement of *M. heureka*

(see LABELING & al. 2008, KÜCK & al. 2011, MOREAU & al. 2013, BOROWIEC & al. 2019). Altogether, the Leptanillinae and Martialinae comprise nine genera and 70 valid species (BOLTON 2020), although generic limits will be subject to revision (BOROWIEC & al. 2019, GRIEBENOW 2020a).

Due to their hypogaecic habits, leptanillines are among the least sampled and studied ants. Live colonies and individuals have been recovered from decaying wood and twigs (BILLEN & al. 2013, HSU & al. 2017), while the cryptic lifestyle and rarity often requires the use of collecting techniques specifically targeting subterranean species, such as “lavage de terre”, mini-Winkler sampling, and hypogaecic pitfalls (LÓPEZ & al. 1994, FISHER 1999, WILKIE & al. 2007, SCHMIDT & SOLAR 2010, WONG & GUÉNARD 2017). All of these methods are more efficient than direct search in the recovery of hypogaecic ants, including species of *Leptanilla* EMERY, 1870 (LÓPEZ & al. 1994, WONG & GUÉNARD 2016) and *Protanilla* TAYLOR, 1990 (MAN & al. 2017). Since the soil is the least explored stratum in the context of Formicidae (AGOSTI & al. 2000), innovative collecting approaches and intensified sampling will certainly lead to new discoveries of hypogaecic species and provide much-needed insight into their biology.

The morphology of Leptanillinae has already received some attention in systematic studies. This includes early contributions of EMERY (1904), the most comprehensive treatment of the subfamily by BOLTON (1990), and some more broadly focused works (e.g., BARONI URBANI & al. 1992, PERRAULT 1999, BRADY & WARD 2005, KELLER 2011, BOUDINOT 2015). Most other studies have been conducted in the context of alpha taxonomy, including those on the relatively recently described genus *Protanilla* (e.g., BOLTON 1990, BHARTI & AKBAR 2013, HSU & al. 2017, MAN & al. 2017, BAIDYA & BAGCHI 2020). Only a few notes have been published on selected internal structures, such as the sting (KUGLER 1992), the tentorium of Iberian *Leptanilla* species (LOPEZ & al. 1994), the mandibular gland of *Leptanilla* (BILLEN & al. 1998), and a detailed investigation of the glandular system of one *Protanilla* species (BILLEN & al. 2013). The morphology of *Opamyрма hungvuong* YAMANE, BUI & EGUCHI, 2008, only recently assigned to Leptanillinae (WARD & FISHER 2016), was studied in some detail, but data on internal structures were restricted to the tentorium (YAMADA & al. 2020). External and internal morphology of male Leptanillinae have been addressed to some degree by, for example, GOTWALD (1969), WHEELER & WHEELER (1930), PETERSEN (1968), BARONI URBANI (1977), KUGLER (1987), OGATA & al. (1995), and BOUDINOT (2015), with the most recent and broadly-sampled study being GRIEBENOW (2020b). Morphological knowledge of *Martialis heureka*, the probable sister group of the Leptanillinae (BOROWIEC & al. 2019), is very limited. The only information on female internal structures of this mysterious species, in particular the sting apparatus, was a consequence of the accidental destruction of the first of only two collected workers (BRANDÃO & al. 2010), while for the male only a gross treatment of the genital

capsule is available beyond external description (BOUDINOT 2015).

Anatomical and behavioral data for *Protanilla* are highly desirable, given that males of the genus are known to display features which may be plesiomorphic for the subfamily, such as the presence of the pterostigma and a reduced ventral cupula in the genitals (GRIEBENOW 2020b). Currently, *Leptanilla* is known to display army-ant-like behavior, including cyclical brood production and a degree of dichthadiigyny (MASUKO 1989, 1990, KRONAUER 2009), and to primarily be a predator of geophilomorph centipedes (OGATA & al. 1995). While *Protanilla* does have a similar diet, it does not appear to have the specialized life cycle of *Leptanilla* (BILLEN & al. 2013, HSU & al. 2017). An intriguing feature, however, is the way in which *Protanilla* open and close their mandibles, suggesting the presence of a trap-jaw mechanism. This is a kind of power-amplified mechanism in which the muscles store potential energy in an elastically deformable spring to then release this through fast release of a latch. This allows much faster movements than the physiological limit of muscles normally would. In contrast to “snapping” power-amplified mechanisms, the mandibles are in an open position when the strike is initialized in trap-jaw ants through release of the latch (LARABEE & SUAREZ 2014, LARABEE & al. 2017). Trap-jaw ants, including *Odontomachus*, *Strumigenys*, and *Myrmoteras*, are among the species with the most intensively studied morphology (e.g., BROWN 1953, GRONENBERG 1995, 1996, GRONENBERG & al. 1998, BOLTON 1999, BARONI URBANI & DE ANDRADE 2007, LARABEE & al. 2017). An opening angle of 180° was documented for *Protanilla* mandibles by Taylor (HÖLLDOBLER & WILSON 1990: 592). Repeated observations have been made since then, including most recently by HSU & al. (2017), who also observed the ants “striking” with their mandibles to grab prey and locking them in opened position when guarding the nest. However, detailed morphological and functional investigations of the articulation and possible trap-jaw mechanism have been lacking so far.

In the present study, we investigate the heretofore unknown head anatomy of *Protanilla lini* in detail. As this species is a representative of the leptanillomorph ants, this study is an important step in the ongoing effort to document the overall variability of cephalic structural features throughout the ant tree of life. We discuss the observed anatomical features with respect to hypogaecic lifestyle, predatory habits, and phylogenetic implications, particularly with respect to possible ground plan conditions of the crown Formicidae. Additionally, we propose a potential mode of movement for the mandible based on micro-computed tomography scans (μ -CT) of heads with closed and opened mandibles of *P. lini* and the very similar species *Protanilla rafflesi* TAYLOR, 1990.

Material and Methods

Material: Nine specimens of *Protanilla lini* were available for this study, of which two were used in μ -CT scanning

Tab. 1: Scanning parameters for micro-computed tomography scans performed with a Zeiss Xradia 510 Versa 3D (Zeiss, Jena, Germany) (CASENT0709417 and CASENT0742972) and Bruker Skyscan 2211 (Bruker, Billerica, USA) (CASENT0790210). Complete scanning parameters are also deposited together with the Scan data at Zenodo (doi: 10.5281/zenodo.4411058).

Species	Taxon code	Body part	Voxel size	Exposure time (s)	Power (W)	Voltage (kV)	Amperage (uA)	Step size (°)
<i>P. lini</i>	CASENT0790210	head	0.5	2.7	0.7	70	350	0.15
<i>P. lini</i>	CASENT0709417	head	0.6712	20	2.73	40.28	67.81	0.18
<i>P. rafflesi</i>	CASENT0742972	head (closed mandibles)	0.8232	30	3	40.27	74.39	0.18
<i>P. rafflesi</i>	CASENT0742972	head (open mandibles)	1.227	3.7	4.02	50.29	79.95	0.18

and scanning electron microscopy, six were used for histology, and one preserved in ethanol as an untouched voucher. Specimens were collected in Yuchih Township, Nantou County, Taiwan, on 7.XII.2015 by Po-Cheng Hsu using hand-collection (see also Hsu & al. 2017) and preserved in 70% ethanol. The specimens not used for histological sections were entirely depigmented and fragile. For μ -CT scans of the *P. lini* heads, two specimens were used (CASENT0709417 and CASENT0790210). As not enough specimens of *P. lini* were available to generate scans with opened mandibles, we used one specimen (CASENT0742972) of *Protanilla rafflesi* TAYLOR, 1990 with the following collecting information: Singapore, Seletar Trail, 1.39 103.8, 0 m asl, collection code MKLW000111, Berlese extraction of soil, secondary forest, 5.III.2016, MKL Wong. Identifications are based on Xu (2012). An overview of the examined specimens is provided in Table S1.

Photomicrography: As the available specimens were almost completely depigmented and transparent, no photomicrographs to document coloration were taken. Data on the color of the cuticle can be found in the taxonomic literature (Hsu & al. 2017).

Micro-computed tomography scanning (μ -CT scanning): μ -CT-scans were obtained of two individuals of *Protanilla lini* and one of *Protanilla rafflesi*. The first specimen of *P. lini* (CASENT0709417 / CTAR0046) was fixed in a defined position within a small piece of a pipette tip, then dehydrated (70, 80, 90, 95, 100% ethanol), and stained with iodine solution (2M) for 18 hours. Afterwards, it was transferred to 100% ethanol, and the severed pipette tip piece was inserted into a complete pipette tip. The head of the specimen was scanned using a Zeiss Xradia 510 Versa 3D X-ray microscope (Zeiss, Jena, Germany) operated with the Zeiss Scout-and-Scan Control System software (version 11.1.6411.17883) at the Okinawa Institute of Science and Technology Graduate University (OIST), Japan. 3D reconstructions of the resulting scan projection data were done with the Zeiss Scout-and-Scan Control System Reconstructor (version 11.1.6411.17883) and saved in DICOM file format. In order to generate data about the mandible opening mechanism, we first scanned the head (with closed mandibles) of the specimen of *P. rafflesi* (CASENT742972) using the same procedure as

described above, with the notable exception that it was not dehydrated. Afterwards, the head was detached from the body and macerated in a 10% KOH solution for six hours until all internal soft tissue was dissolved. The head was then washed in a 6% acetic acid solution for about 10 hours and then transferred into a petri dish with 100% ethanol. The mandibles were then carefully manually opened with very fine forceps up to the maximum opening gape. The head was removed from the ethanol and dried for a few minutes while making sure that the mandibles stayed in their position. The final preparation step was to mount the head on a triangular paper tip before μ -CT-scanning. Both specimens scanned at OIST are deposited in the collection of that institution. Scanning parameters can be found in Table 1. The second specimen of *P. lini* (CASENT0790210 / CTAR0047), displaying a protracted maxillolabial complex, was first prepared in the same way as described above for *P. lini* (CASENT0709417 / CTAR0046). However, after staining in iodine solution, it was transferred into 100% acetone and dried at the critical point in liquid CO₂ with an Emitech K 850 Critical Point Dryer (Sample Preparation Division, Quorum Technologies Ltd., Ashford, England). The dried specimen was scanned with a Bruker Skyscan 2211 μ -CT-Scanner (Bruker, Billerica, USA) at the Max Planck Institute for the Science of Human History in Jena, equipped with a high resolution (4000 × 2600 pixel) X-ray sensitive CCD camera. The nanofocus mode was employed in a 360° scan with 0.15° rotation steps. The tomographic reconstruction was done in NRecon (Version: 1.7.3.1) and exported as a 16-bit TIFF image series. This specimen is deposited in the collection of the Phyletisches Museum Jena.

3D modelling and 3D prints: The scan of CASENT0709417 / CTAR0046 was completely segmented and the scan of CASENT0790210 / CTAR0047 was used for a complete volume rendering. Segmentation was performed in Amira 6.0 (Visage Imaging GmbH, Berlin, Germany). The cuticle was pre-segmented by manually segmenting every 30th slice and subsequently semiautomatically segmented using Biomedisa (LÖSEL & HEUVELINE 2016, LÖSEL & al. 2020). All other structures were segmented using the brush tool, magic wand, and the interpolation function of Amira. The resulting segmentations were exported with the plugin script “multiExport”

(ENGELKES & al. 2018) in Amira 6.1 as Tiff image stacks. The image series were then imported in VG-Studio Max 2.0 (Volume Graphics GmbH, Heidelberg, Germany) to create volume renderings (Phong) of individual structures. Additionally, the head capsule and mandibles were exported as surface renderings (.stl) from Amira and 3D printed to get models with movable mandibles using an objet350 (Stratasys, Rehovot, Israel) and an Ultimaker S5 (Ultimaker, Utrecht, Netherlands).

From the first scan (closed mandibles) of CASENT-742972 (used for the assessment of the mandible opening mechanism) the head capsule and both mandibles were manually segmented with Amira 6.5.0. Each segmented object and also the entire head (including mandibles) were exported as a 3D surface in .ply format. From the second scan (open mandibles) only the entire head was exported as 3D surface in .ply format.

The 3D graphics software Blender 2.81 (Blender Foundation, Amsterdam, Netherlands) was used to create an initial arrangement of CASENT742972 (*Protanilla rafflesii*), the specimen for which data with opened and closed mandibles were available. From this state, the individually segmented mandible was moved from the closed into the open state and the mandible rotational axis inferred from the transformation parameters using the Blender Python API. The rotational axis served as a baseline for the inferred movement. The intermediate steps were then refined from observations made with the help of the 3D prints, accounting for collisions of the mandible and head meshes. These steps were subsequently applied to CASENT0709417 (*Protanilla lini*), the inferred mandible motion animated, and additionally images of the mandible in open position were rendered. This approach, importantly, is not a reconstruction of the precise kinematics of the *Protanilla* mandible. Rather it represents a hypothesis (or “educated guess”) of the mandibular movement based on interpolation between the (artificial) open and closed positions while taking articulation morphology into account (Videos S1 & S2, as digital supplementary material to this article, at the journal’s web pages). Additionally, the 3D prints were used to experiment on the mandible opening mechanism and using a Samsung Galaxy S9 camera (Samsung Electronics GmbH, Schwalbach, Germany) some of those trials were documented and edited into Video S3 with Adobe Premiere Pro 2020 (Adobe System Incorporated, San Jose, USA).

Scanning Electron Microscopy (SEM): The critical point dried specimen of *Protanilla lini* previously used for μ -CT scanning (CASENT0790210 / CTAR0047) was glued on the tip of a minute needle laterally on its metasoma. It was subsequently sputter coated with gold using an Emitech K 500 (Sample Preparation Division, Quorum Technologies Ltd., Ashford, England). A rotatable specimen holder (POHL 2010) was employed to take SEM micrographs of the head from all directions, using a Philips ESEM XL30 (Philips, Amsterdam, Netherlands) equipped with Scandium FIVE software (Olympus, Münster, Germany).

Histological section series: To create a large posterior opening for the penetration of the various chemicals used during tissue processing, the posterior third of the head was severed with a transverse cut. The heads were then fixed in 2% cold glutaraldehyde in a buffer of 50 mM Na-cacodylate and 150 mM saccharose. Postfixation with 2% osmium tetroxide was carried out in the same buffer, followed by dehydration in a graded acetone series. Tissues were embedded in Araldite® and sectioned with a Leica EM UC6 ultramicrotome (Leica, Wetzlar, Germany). Two heads each were embedded in transverse, longitudinal and frontal orientation. Serial semithin sections were performed with a thickness of 1 μ m. The sections were stained with a 0.1% solution of methylene blue and thionin and viewed under an Olympus BX-51 microscope (Olympus, Tokyo, Japan), equipped with an Olympus Camedia C-3040 Zoom digital camera. The 20 \times objective was employed to take images at 10 μ m intervals, and additional images of anatomical details were taken with a 40 \times objective and a 100 \times objective with immersion oil. Images were used for anatomical comparison and descriptions. Selected section images were mounted as image plates as described below.

Measurements: In order to quantify setation length and density on the cranial surface, Photoshop was used to measure the minimum distance between 48 seta insertions, the length of 18 “microsetae”, and seven “macrosetae” from Figure 1B (SEM). Seta length was measured linearly from base to tip, thus represents an underestimate of the total length as all quantified setae were curved to some degree.

As sarcomere length has previously been shown to be an important indicator of muscle fiber performance (PAUL & GRONENBERG 1999), we measured this for **M. craniomandibularis internus** (Omd1). Because the frontal sections available were not of ideal quality and not prepared specifically for this purpose, the validity of these results is limited. However, they are in a similar range of variation compared with previous analyses (PAUL & GRONENBERG 1999). On each of three directly attached and four thread-attached fibers, ten randomly selected sarcomeres were measured using ImageJ (SCHINDELIN & al. 2012). Measurements were taken from the center of one dark band to the next. Measurements and calculated average sarcomere lengths can be found in Table S2, and the images used to measure sarcomere length in Figure S1.

Finally, using Amira and Biomedisa, we segmented the left **M. craniomandibularis internus** (Omd1) of one specimen (CASENT0709417) and estimated muscle architecture parameters. To account for tissue shrinkage affecting muscle volume, we additionally segmented the empty space between muscle fibers and estimated muscle volume based on the number of segmented voxels multiplied with voxel size. After masking the tomogram with the segmentation, we traced individual muscle fibers with modules from the Amira XTracing extension, which yields number of fibers, fiber lengths, and location of the fibers.

With a custom script using Python in Blender 2.81, we vectorized the fibers and estimated individual pennation angles towards the apodeme (J. Katzke, P. Puchenkov & E.P. Economo, unpubl.), and calculated the average attachment angle. The detailed results of the fiber analysis are available on Zenodo (DOI 10.5281/zenodo.4411058) in the file “Protanilla lini_CASENT0709417_mandibular_adductor_fiber_analysis.zip”.

Data availability: The μ -CT scans used in this study are available at the online repository Zenodo under the DOI 10.5281/zenodo.4411058.

Image processing: Image plates were arranged in Adobe Photoshop® CS6 (Adobe System Incorporated, San Jose, USA). All images were subjected to limited levels adjustment and smart sharpen (30%). Labels for the image plates were created in Adobe Illustrator® CS6 (Adobe Systems Incorporated, San Jose, USA).

Terminology: The terminology follows RICHTER & al. (2020). Being prognathous, the cranium of female ants is oriented along the craniocaudal axis of the body (“longitudinal axis”), with the facial or frontal surface being dorsal, and the ventral surface of the head comprising the postgenal bridge. We refer to “full-face view” when the anteriormost and posteriormost margins of the cranium are in the same plane of focus, and consequently the dorsal surface is referred to as the “frontal surface”. We define the coordinate system of the antenna assuming that the appendage is directed away from the prognathous cranium, that is, dorsally, such that the surface closest to the mouth is “anterior”, and that surface directed closest to the posterior head margin is “posterior”. For the maxillolabial complex, a retracted position is considered as standard condition. The anterior lateral projection of the hypostoma was termed “hypostomal tooth” in the Hymenoptera Anatomy Ontology (HAO_0000416), and we adopt this terminology here to better differentiate these projections from the “triangular hypostomal processes”. We recognize the differentiated thick setae on the aboral surface of the labrum and the ventromedial surface of the mandibles as “chaetae”, or **sensilla trichodea chaetiformis**, in distinction to thin, longer “setae”, or **sensilla trichodea setiformis** (BOUDINOT & al. 2020b; chaetae also known as “traction setae”, e.g., BOLTON & FISHER 2008; or “peglike setae”, e.g., KELLER 2011; or “spicules”, e.g., BARDEN & GRIMALDI 2013). Where distinct, dense patches of short **sensilla trichodea** occur on proximal contact surfaces, these are termed “proprioceptor seta patches” (KELLER 2011). Terminology for setation stature follows WILSON (1955).

Results

Head capsule, external: The pronouncedly prognathous head of workers of *Protanilla lini* is slightly longer than broad; in dorsal view, the lateral margins are slightly convex but nearly parallel in the middle region of the head capsule; the posterior cephalic margin is almost straight; in lateral view, the head appears elongated oval (Figs. 1A - C; 2). The occipital region is countersunk (concave) and

completely surrounded by an occipital carina (oca, Figs. 1C, F; 2D); the postocciput is mushroom-shaped with a broader dorsal portion (pocc, Fig. 2D); it encloses the hourglass-shaped narrow occipital foramen; the orientation of the foramen on the posteriormost part of the head is almost in direct opposition to the oral foramen, thus aligned with the longitudinal axis of the cranium. The postgenal ridge is externally marked by a very shallow furrow and by the absence of sensilla trichodea or trichia along the midline of the postgenal bridge (pgb, Figs. 1C; 2B). The large clypeus appears trapezoidal in dorsal view (cl, Figs. 1A; 2A); the posterior clypeal margin at the level of the posterior margin of the antennal toruli is almost straight; the anterior margin is slightly emarginate; the middle portion of the clypeus is distinctly raised compared with the surrounding areas of the head capsule; it appears evenly curved in lateral view; the raised portion of the clypeus forms an almost right angle with the surrounding lateral clypeal regions; the anteriormost clypeal surface is inflected posteroventrally, and the distolateral edges protrude anteriorly over the dorsal mandibular bases (Figs. 1A, B; 2A, C); the lateral part of the clypeus forms the cranial condyle of the dorsal (secondary) mandibular articulation (dma, Fig. 2C); the laterodistal clypeal edges form small knobs (dck, Figs. 1A, B; 2A, C; 3A) articulating with a dorsal furrow of the mandibular base (see **Mandible** below); the main part of the articulation is separated from the distal knob by a straight horizontal margin; it is formed by a second knob (dma, Figs. 1A, B; 2A, C; 3A) directly anterad / dorsad the large acetabulum of the ventral mandibular articulation (vma, Fig. 3A). A supra-clypeal area (“frontal triangle”) is not visible externally. Frontal carinae are not expressed. The antennal toruli are simple ring-shaped elevations with a slightly oblique orientation relative to the sagittal plane (formed by the dorsal and longitudinal axes) of the head capsule (i.e., toruli directed dorsolaterally assuming prognathy) (to, Figs. 1A, B; 2A, C; 4A; 5C); the cuticle surrounding them is only slightly countersunk (Fig. 5C). The anterior tentorial pits are located directly anterolaterad the antennal toruli (atp, Fig. 5C). Compound eyes and ocelli are absent. The hypostomal carina is raised from the surrounding cuticle, thus forming a thick wall-like structure surrounding the buccal cavity on the ventral side (hysc, Figs. 1B, C; 2B; 3A); a deep hypostomal cavity, containing the base of the maxillolabial complex at rest, is present (hyc, Figs. 3A; 6D); the hypostomal teeth are long, extending ventrally over the mandibular bases (hyt, Figs. 2B; 3A); their triangular tips correspond to the thick triangular hypostomal processes (hysp, Figs. 3A; 4B; 6D), which separate the mandibular foramina from the remainder of the oral foramen; medially, these processes form a distinct edge with the surface of the hypostomal cavity, which receives the lateral stipital edges (*, Fig. 3A). The cuticle of the head is very smooth, with a subtle microrugosity only visible at high magnification (Fig. 1A - C, E), not conforming to the underlying cell structure as observed elsewhere (Fig. 1F). The surface of cranium with two co-expressed classes of

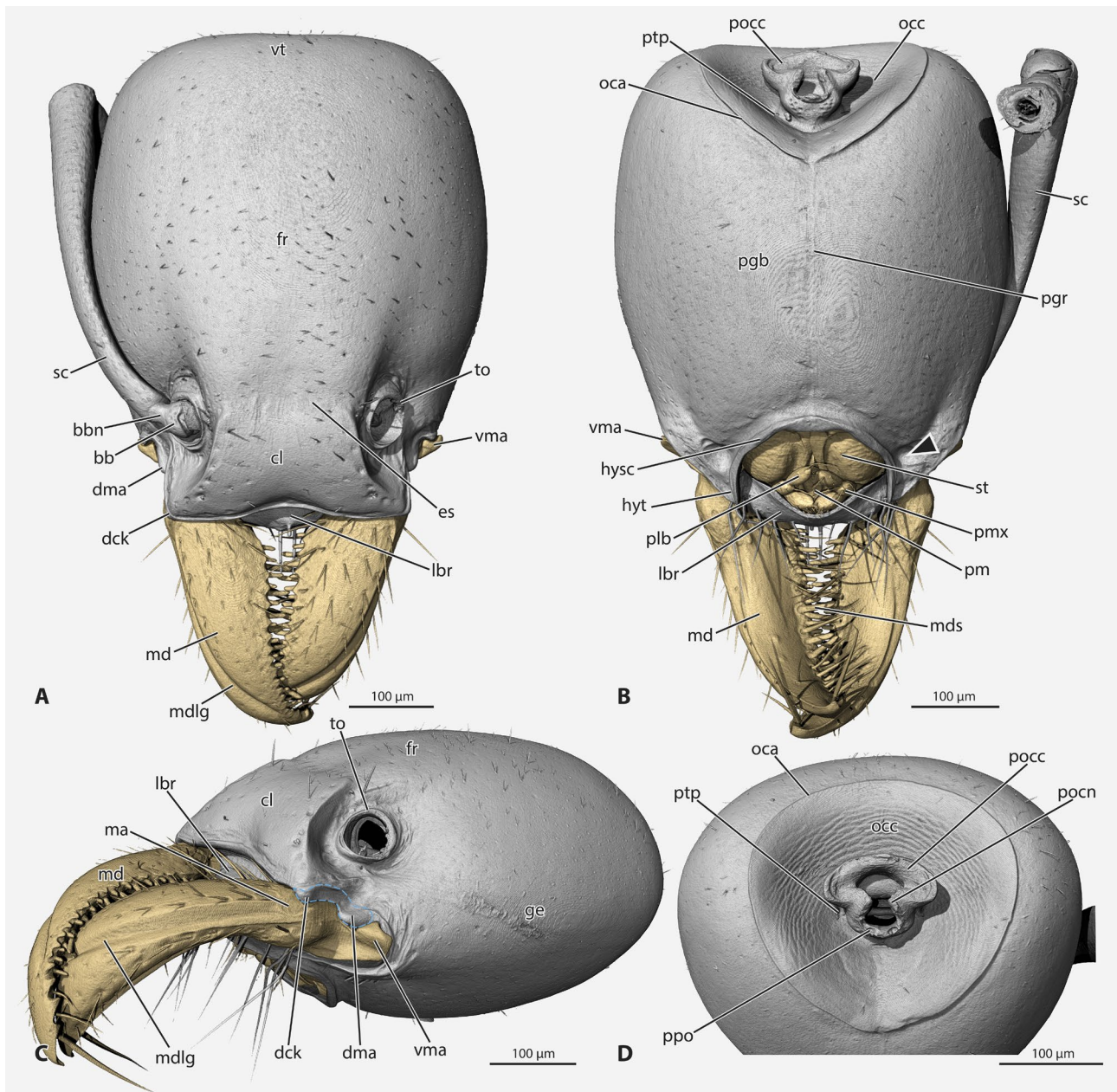


Fig. 2: Volume renderings of the head of *Protanilla lini*. **A:** Overview, dorsal view. **B:** Overview, ventral view. **C:** Overview, frontolateral view. **D:** Occipital area, posterior view. **Abbreviations:** **bb** – bulbus; **bbn** – bulbus neck; **cl** – clypeus; **dck** – distal clypeal knob; **dma** – dorsal mandibular articulation; **es** – epistomal sulcus; **fr** – frontal area; **ge** – genal area; **hyt** – hypostomal tooth; **hysc** – hypostomal carina; **lbr** – labrum; **ma** – mandalrus; **md** – mandible; **mdlg** – lateral mandibular groove; **mds** – mandibular sensilla trichodea; **oca** – occipital carina; **occ** – occipital area; **pgb** – postgenal bridge; **pgr** – postgenal ridge (visible as slight sulcus); **plb** – labial palp; **pmx** – maxillary palp; **pm** – prementum; **pocc** – postocciput; **pocn** – postoccipital condyle; **ppo** – posterior process opening; **ptp** – posterior tentorial pit; **sc** – scapus; **st** – stipes; **to** – torulus; **vma** – ventral mandibular articulation; **vt** – area of the vertex. **Colors:** beige / brown – mouthparts; grey – cuticle. **Symbols:** black arrowhead – depression close to tip of postgenal carina; blue outline – clypeal condyle of the dorsal mandibular articulation.

(dta, Fig. 6D) at the level of the posterior end of the mesal lamella are distinctly developed; a broad base is followed by a short, relatively thick tube-like part facing anterad with a diagonal orientation. A secondary tentorial bridge is missing. Posterior tentorial processes are present as very short tubes in the posterior ventral postoccipital region (pp, Fig. 6D). The postgenal ridge (pgr, Fig. 6B) is wide

anteriorly and narrows posteriorly; the posterior end splits up, and the two sides connect to the posterior tentorial arms (Fig. 3A). The internal parts of the toruli are simple rings with a flat edge (to, Fig. 6D), distinctly thickened anteroventrally and lacking a distinct internal process (torular apodeme). The broad, flat, and rounded epistomal ridge (esr, Figs. 6B; 10C) follows the clypeal outline, with a

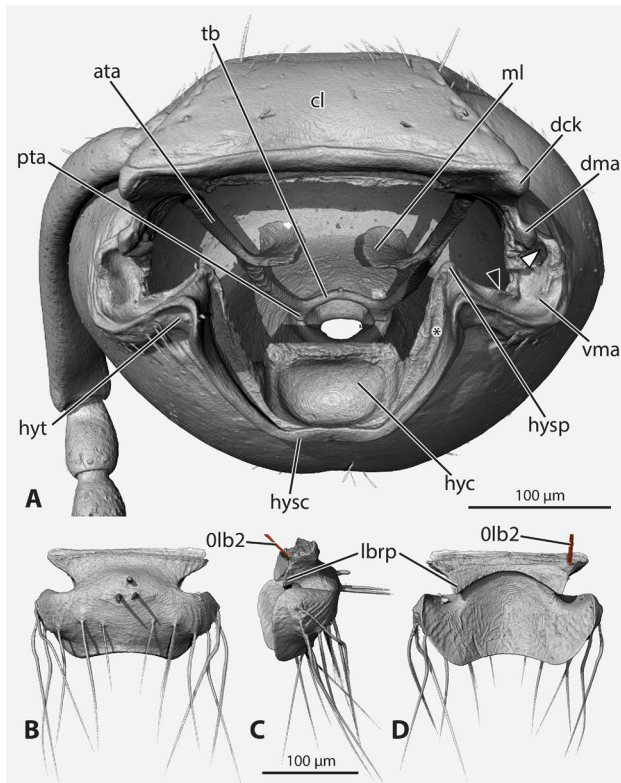


Fig. 3: Volume renderings of the head of *Protanilla lini*. **A:** Head capsule without mouthparts, frontal view. **B - D:** Labrum, B: frontal, C: lateral, and D: posterior view. **Abbreviations:** **0lb2** – *M. frontoepipharyngalis*; **ata** – anterior tentorial arm; **cl** – clypeus; **dck** – distal clypeal knob; **dma** – dorsal mandibular articulation (second / main clypeal knob); **hyt** – hypostomal tooth; **hyc** – hypostomal cavity; **hysc** – hypostomal carina; **hysp** – hypostomal process; **lbrp** – lateral labral process; **ml** – mesal tentorial lamella; **pta** – posterior tentorial arm; **tb** – tentorial bridge; **vma** – ventral mandibular articulation (cranial acetabulum). **Colors:** grey – cuticle. **Symbols:** black arrowhead – carina at the central posterior margin of the cranial acetabulum; light grey arrowhead – notch between clypeal condyle and hump of the acetabulum; * – edge of the hypostomal process receiving the lateral margin of the stipes.

straight posterior line visible externally; it curves anterad around the internal toruli and is fused to the deep clypeal inflection in this region; laterally, it reaches the dorsal edge of the ventral (primary) acetabulum of the mandible. Additionally, a broad, flat ridge is present along the midline of the clypeus (*mcr*, Figs. 6B; 10C).

Labrum: Deep lateral grooves divide the labrum into a broad basal portion and an even broader main shield (Figs. 3B - D; 4A, C). The straight proximal margin is broadly connected with the inflected clypeal margin (Fig. 6B). The proximolateral corners of the internal labral wall bear short, ventrally curved triangular processes (*lbrp*, Fig. 3C, D); their hook-like tips contact the first maxillary palpomere dorsally (Fig. 4A). The deep lateral grooves receive the dorsomedial margin of the mandible (Fig. 4C). The main shield is broadly convex and covers

the distal part of the maxillolabial complex in its resting position (Figs. 2B; 4A). Due to the distinctly concave distal margin, the labrum appears bilobed; the aboral (external) surface is largely smooth, except for some rugose proximolateral areas; three conspicuous and thick sensilla trichodea chaetiformis are situated medially at the level of the lateral grooves (Fig. 3B–D), the proximomedial chaeta is short and blunt, while the distolateral pair of differentiated setae are longer, pointed, circa 1 / 3 the length of the more distal setae, and are stiff and bristle-like; the proximomedial chaeta has the same ridged surface structure as those traction chaetae on the ventral side of the mandibles (Fig. 1D); additionally, several long, thin and pointed setae inserted along the mid-level of the main labral shield are directed distally, whereas the three thick sensilla trichodea point directly away from the labral surface (Fig. 3B–D).

Musculature (Figs. 3C; 10A, C, D). **M. frontoepipharyngalis (M. 9 / 0lb2)**, rather large muscle; Origin (= O): frontal area shortly posterad the antennal bases, laterad *0bu2* and *0bu3* (Fig. 10C); Insertion (= I): with a long tendon on the proximolateral labral wall, laterad the triangular processes of the internal wall (Fig. 3C).

Antennae: The 12-segmented geniculate antennae are inserted very close to the anterior edge of the head as seen in full-face view, at the level of the primary (ventral) mandibular articulation (Figs. 1A, B; 2A, 4A, 5B); their dorsolaterally placed and nearly vertically oriented foramina are widely separated by the clypeus. The bulbus is semicircular (*bb*, Fig. 5C) and almost completely exposed in dorsal view; anteriorly it articulates with the long and thin antennifer (*ant*, Fig. 4A); the bulbus neck is short and straight (*bbn*, Fig. 5C). The scapus is slightly curved in its proximal third and slightly shorter than the flagellum (*sc*, Fig. 5A, B). The base of the pedicellus (*pd*, Fig. 5A) is moderately curved anterad. The flagellomeres increase slightly in length and width apically (Fig. 5A); the apicalmost one is the longest and broadest, tapers distally, and is apically pointed. All antennomeres bear a dense appressed to subdecumbent pubescence and more dilute appressed to erect pilosity; all setae of the scapus are thin and pointed; the surface of the bulbus bears a proprioceptor patch of microsetae; the pattern of setal length, orientation and arrangement varies distinctly from the proximal to the distal antennal region (Fig. 5A, B).

Musculature (Fig. 6A, B). Due to the orientation of the tentorial lamella and the anterior location of the antennal insertion, the orientation of the extrinsic scapal muscles is almost parallel to the longitudinal axis of the head. **M. tentorioscapalis anterior (M. 1 / 0an1)**: O: anterolateral surface of the mesal tentorial lamella; I: on a tendon inserting anteriorly on the bulbus. **M. tentorioscapalis posterior (M. 2 / 0an2)**: moderately flattened dorsoventrally; O: posterior / dorsal edge of the mesal lamella of the anterior tentorial arm; I: tendon inserted posteriorly on the bulbus. **M. tentorioscapalis lateralis (M. 3 / 0an3)**: largest extrinsic muscle; O: anterior tentorial arm laterad the other muscles and on the entire dorsal tentorial arm; I: tendon inserted laterally on the bulbus.

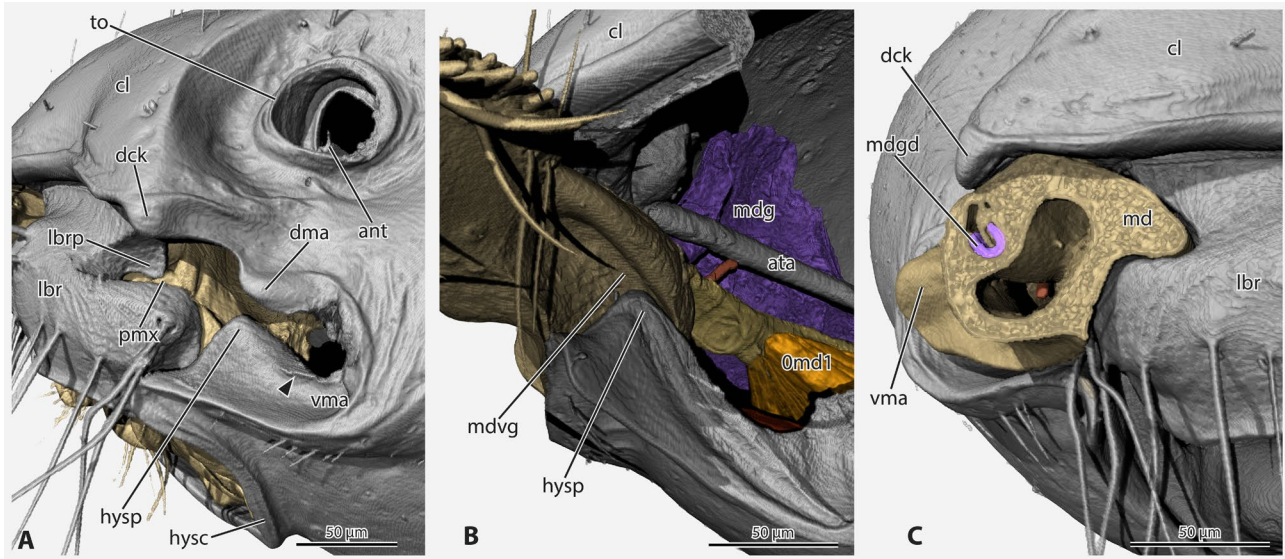


Fig. 4: Volume renderings of the head of *Protanilla lini*. **A:** Anterior head capsule with removed mandible showing its articular area, frontolateral view. **B:** Anterior head capsule with all mouthparts except removed mandible, mesoventral view. **C:** Head with mandible cut to show interaction of mandible and lateral labral groove, frontal view. **Abbreviations:** **0md1** – M. craniomandibularis internus; **ant** – antennifer; **ata** – anterior tentorial arm; **cl** – clypeus; **dck** – distal clypeal knob; **dma** – dorsal mandibular articulation (second / main clypeal knob); **hysc** – hypostomal carina; **hysp** – hypostomal process; **lbr** – labrum; **lbrp** – lateral labral process; **md** – mandible; **mdg** – mandibular gland; **mdgd** – mandibular gland duct; **mdvg** – ventral mandibular groove; **pmx** – maxillary palp; **to** – torulus; **vma** – ventral mandibular articulation (cranial acetabulum). **Colors:** **beige / brown** – mouthparts; **grey** – cuticle; **orange / red** – muscles; **purple** – glands. **Symbols:** black arrowhead – carina at the central posterior margin of the cranial acetabulum.

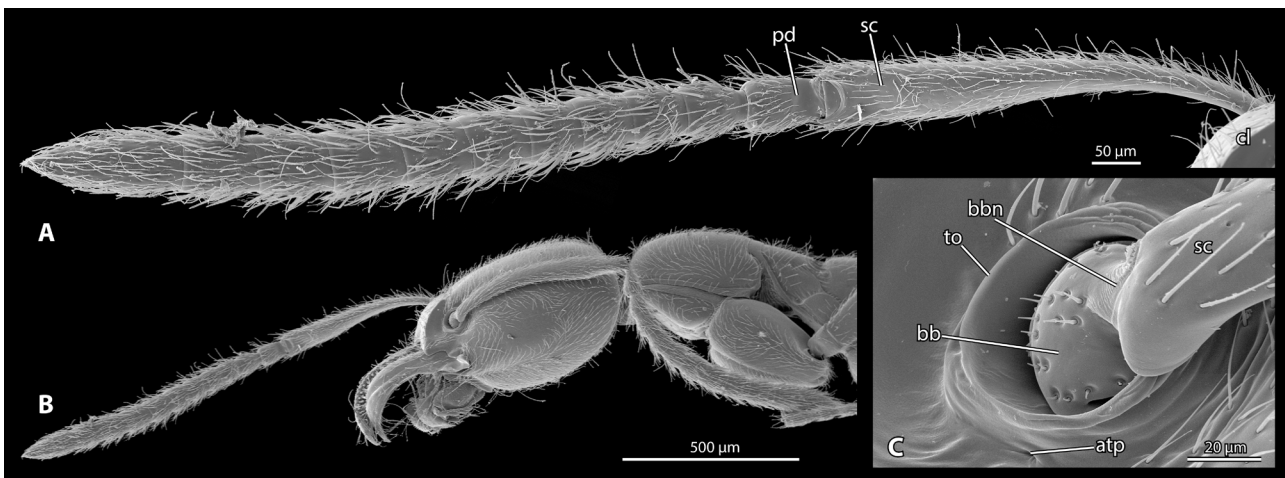


Fig. 5: Scanning Electron Microscopy micrographs of the antenna of *Protanilla lini*. **A:** Right antenna fully extended, medial view. **B:** Overview of the head with both antennae extended, lateral view. **C:** Detail of the antennal insertion. **Abbreviations:** **atp** – anterior tentorial pit; **bb** – bulbus; **bbn** – bulbus neck; **cl** – clypeus; **pd** – pedicel; **sc** – scapus; **to** – torulus.

M. tentorioscapalis medialis (M. 4 / 0an4): O: along the mesal edge of the mesal lamella of the anterior tentorial arm, mesad the other muscles, surrounding 0an1 mesally; I: tendon inserted mesally on the anterior region of the bulbus. **M. scapopedicellaris lateralis (M. 5 / 0an6),** O: ventrally on the scapus; I: short tendon on the ventral base of the pedicellus. **M. scapopedicellaris medialis (M. 6 / 0an7):** O: anteriorly on the distal fourth of the scapus; I: long tendon on the dorsal base of the pedicellus.

Mandibles: The mandibles are more than three times as long as broad (md, Figs. 6C, D; 7A, D). The basal stem is about a third as long as the total length, and almost as broad as the base of the main mandibular sub-unit, the blade. The blade appears elongate triangular in dorsal view, and the distal half strongly bent downwards (visible in lateral view, Figs. 6D; 7A); the medial masticatory edge proximally forms a gentle curve with the short basal margin (bm, Figs. 6C; 7D), which is con-

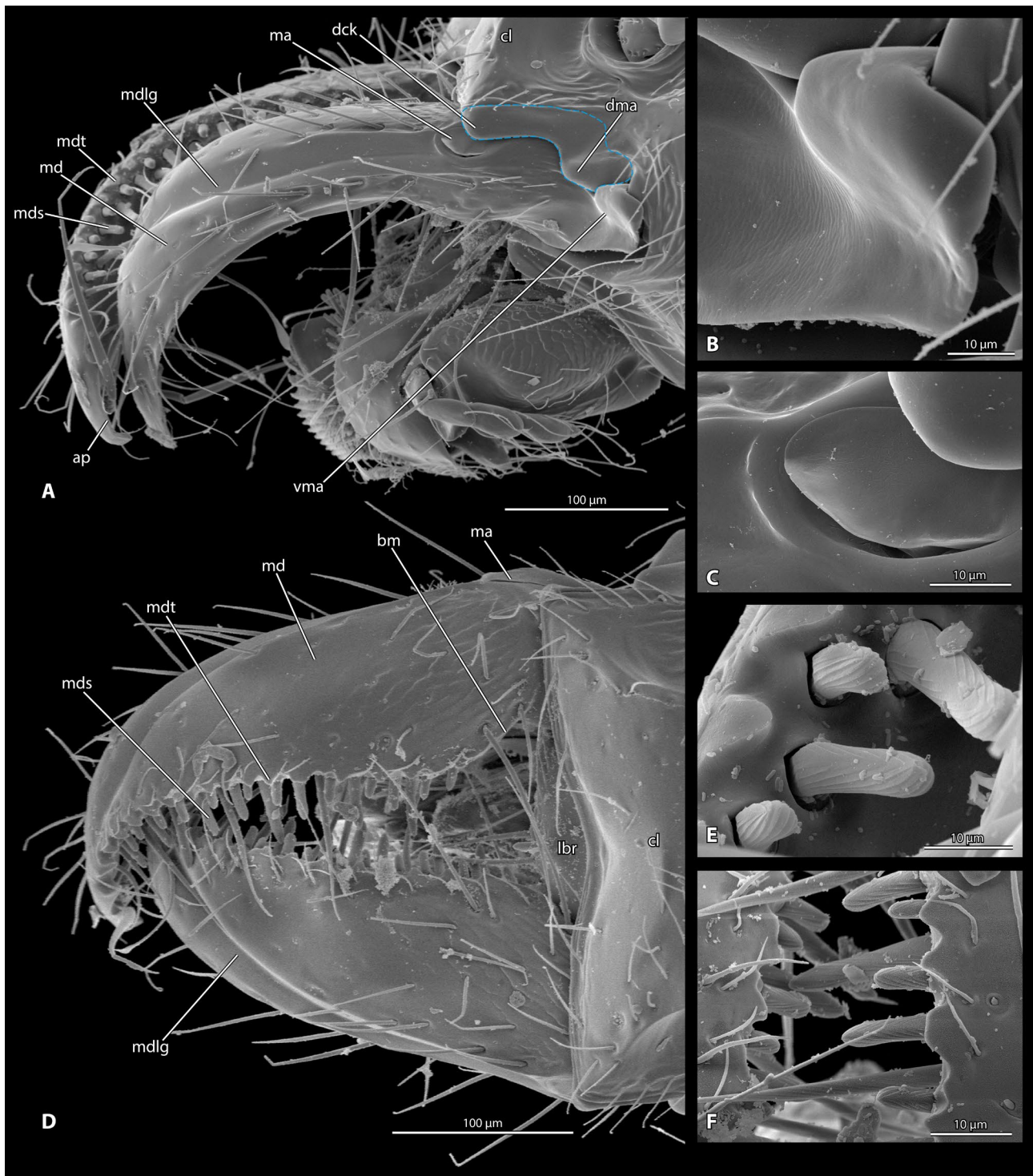


Fig. 7: Scanning Electron Microscopy micrographs of the mandibles of *Protanilla lini*. **A - C, E:** Lateral view. **D, F:** Dorsal view. **A, D:** Overview of the mandibles. **B:** Detail of the ventral articular process formed by fused atala and ventral (primary) mandibular condyle. **C:** Detail of the mandalus. **E, F:** Detail of the traction setae. **Abbreviations:** **ap** – apical tooth / apical blade; **bm** – basal margin; **cl** – clypeus; **dck** – distal clypeal knob; **dma** – dorsal mandibular articulation; **lbr** – labrum; **ma** – mandalus; **md** – mandible; **mdlg** – lateral mandibular groove; **mds** – mandibular sensilla trichodea; **mdt** – mandibular tooth; **vma** – ventral mandibular articular process; **Symbols:** blue outline – area of the clypeal condyle of the dorsal (secondary) mandibular articulation.

A deep groove extends along the dorsolateral side of the blade over most of its length. It traverses anteriorly towards the masticatory margin and ends behind the

fourth tooth (mdlg, Fig. 7A, D). The ventral margin of the mandible bears a long carina that extends to the apical tooth (mdc, Fig. 6C).

The basal stem forms the highly complex articular surfaces with the head capsule. The dorsal groove on the blade continues as an oblique tunnel extending through the dorsolateral mandibular base; it contains the duct of the mandibular gland (mdgd, Fig. 4C), which opens at the base of the lateral mandibular groove at a membranous field representing the anteriorly shifted mandalus (ma, Figs. 6C; 7A, C, D). A mesally widening, flat oblique furrow is visible above the oblique tunnel; it reaches the mandalus laterally on the dorsal side of the mandibular base (black arrow, Fig. 6C); the furrow is in contact with the distolateral clypeal knob (dck, Figs. 4A, C; 7A, D). Manipulation of 3D prints and animations revealed that the knob slides across the furrow in the opening phase and loses contact with the mandible as the gape widens (Videos S1, S3, S4, S5).

The main clypeal condyle (dma, Figs. 4A; 7A) is located further posterior and corresponds to the main articular surface of the dorsal (secondary) mandibular acetabulum, which is small and broader than long (dma, Fig. 6C). In other ants, this surface is larger and defines the articulation on the dorsal side, whereas in *Protanilla* the whole area between the two clypeal knobs is involved in the mandibular articulation (marked area, Fig. 7A).

The region corresponding to the atala in other ants, marked by the insertion site of the tendon of the *M. craniomandibularis externus* (Omd3) (Fig. 6C), and the ventral mandibular condyle are fused into a single articular process (vma, Figs. 6C; 7A, B). The process extends laterally beyond the head capsule (vma, Figs. 1A; 2A; 4C). It rests in a large ventral articular acetabulum of the cranium and dorsally bears a small groove on its posterior side corresponding to a hump of the acetabulum (vma, Figs. 3A; 4A); in the resting position, this hump and groove lock into each other closely, with the process protruding around the head capsule (Fig. 7B); a medial carina forms a sharply defined border of the acetabulum (black arrow, Figs. 3A; 4A).

A thick strengthening ridge along the medial side of the entire mandibular base articulates with the deep labral groove (Fig. 4C); on the ventral side, it forms a deep groove interacting with the triangular hypostomal process (mdvg, Figs. 4B; 6C).

In the closed position, we observed that the protruding articular process and the deep ventral groove lock the mandible tightly in 3D printed models. In the open position, the process rests in a notch between the main clypeal condyle and the hump of the acetabulum (light grey arrow, Fig. 3A). In the open position, the mandibular gape is around 180°, and only dorsal mandibular acetabulum and articular process remain in direct contact with the head (Videos S1, S5).

The cuticle of the mandible is largely smooth; microrugosity, not reflecting cellular boundaries, is recognizable on the surface anterad the laterally projecting ventral condyle (Fig. 7B).

Musculature (Fig. 6C, D). ***M. craniomandibularis internus* (M. 11 / Omd1)**: largest cephalic

muscle; O: posterior halves of the posterior, ventral, and lateral inner surfaces of the head; a bundle dorsolaterad the occipital foramen is isolated; I: the adductor tendon with a thick, round main piece connects to the dorsomesal mandibular base with a flattened, dorsoventrally oriented ligament; posteriorly, a long main branch is distinctly flattened and reaches about the middle region of the head capsule as a slightly oblique sheet; a dorsal accessory branch originating from this sheet-like part is the attachment area of the isolated muscle bundle; the posteriorly originating muscle fibers (except the occipital bundle) connect directly to the tendon, whereas the anterior ones on the lateral and especially the ventral side attach via thin cuticular fibrillae to the main apodemal body; the directly connecting fibers have shorter sarcomeres than the thread attached ones (average of 2.89 μm vs. 4.74 μm , Table S2), and all fibers attach with very low angles, many running almost parallel to the apodeme (average attachment angle of 23.06°). ***M. craniomandibularis externus* (M. 12 / Omd3)**: a somewhat flattened triangular muscle; O: ventromesal head capsule and postgenal ridge in the anterior half of the head; I: with a relatively long, thin tendon dorsally on the ventral mandibular articular process, on the part corresponding to the atala in other ants; due to the angle of insertion, the muscle has an inward and downward pull. ***M. hypopharyngo-mandibularis* (M. 13) / *M. tentorio-mandibularis medialis inferior* (Omd8)**: extremely thin, scarcely recognizable; O: ventrally on the anterior tentorial arm; I: mediadorsally on the inner mandibular surface.

Maxillae: The maxillae are of a generalized formicid form in their overall configuration (Figs. 8; 9E - G). The external stipital sclerite is broadly oval to rectangular, with a groove along the medial and distal edges, which partly receives the maxillary palp in its resting position (stg, Fig. 8A); the thick margin of the sclerite mediad the groove broadens into a flange on the proximal stipital third; distally, a groove on the medial stipital margin receives the base of the labial palp in retracted position (white arrow, Fig. 8G). The well-developed internal stipital sclerite (sti, Fig. 12A) connects to the stipitopremental conjunctivum (spc, Fig. 12A, C). The four-segmented maxillary palp inserts medially on the distal margin of the external stipital sclerite (pmx, Fig. 8A - C, G); palpomere 1 is cylindrical and slightly flattened, and thus structurally adapted to the tight space delimited by the other mouthparts in resting position; palpomere 2 is also flattened, whereas the other segments are short, club-shaped, and slightly overlapping with each other; few long, thin setae are inserted on each palpomere, most of them on the apical one; palpomere 1 additionally bears several minute cone-shaped proprioceptor sensilla (Fig. 8B). The galea (ga, lc, Fig. 9 E - G) is rectangular with a rounded apex; the lacinia appears almost square in ventral view; the galea is sparsely covered with thin setae dorsally (ga, Fig. 8G); more densely arranged thin setae of varying length on the apical region form the galeal crown, which also bears one distinct, thick chaeta on its medial side (gams, Fig. 8G); the ventral side

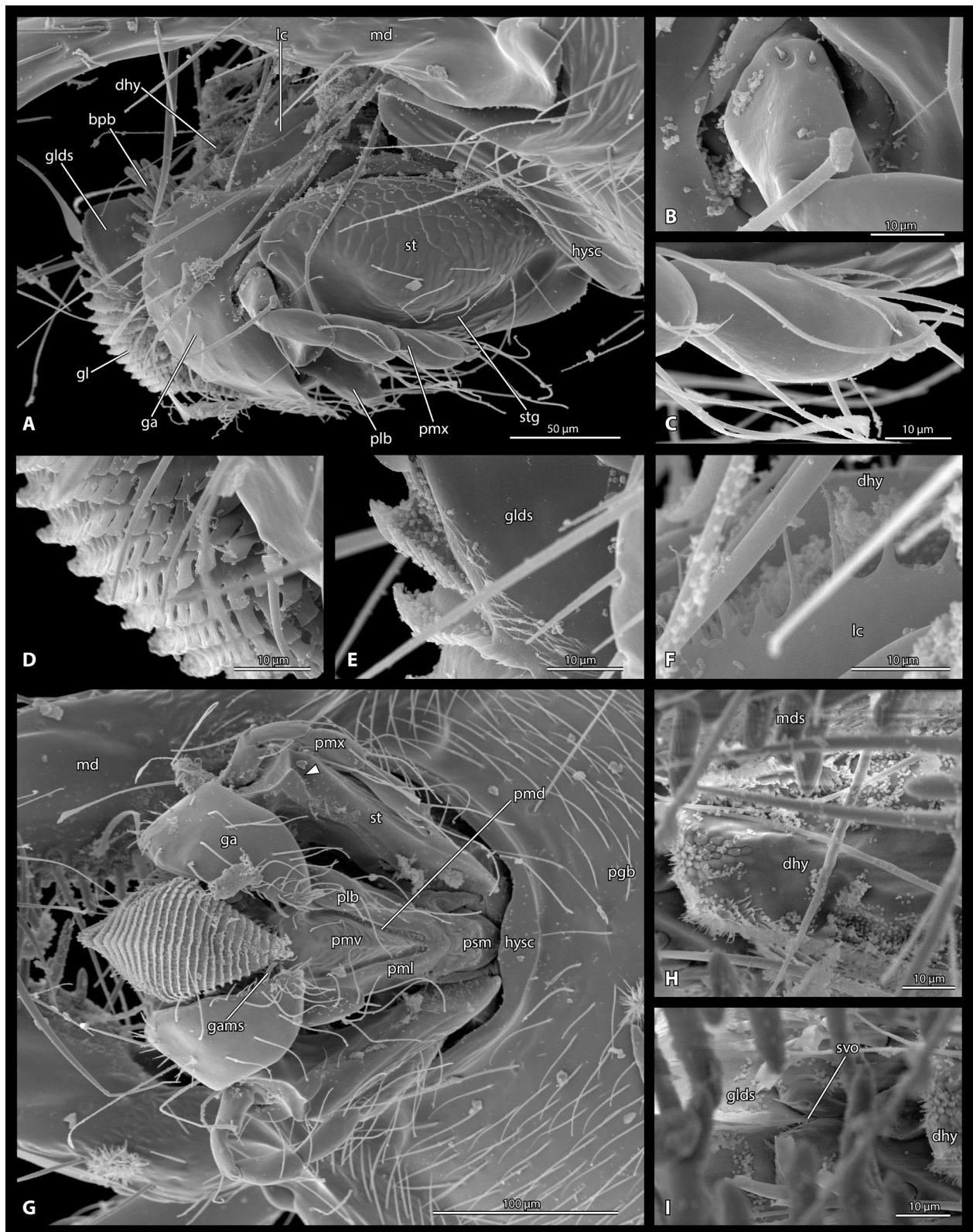


Fig. 8: Scanning Electron Microscopy micrographs of the maxillolabial complex of *Protanilla lini*. **A - F**: Lateral view. **G**: Ventral view. **H, I**: Dorsal view. **A, G**: Overview. **B**: Basal maxillary palpomere. **C**: Distal maxillary palpomere. **D**: Glossal surface. **E**: Dorsal surface of the glossa. **F**: Lacinial crown. **H**: Distal hypopharynx. **I**: Salivary opening. **Abbreviations**: **bpb** – basiparaglossal brush; **dhy** – distal hypopharynx; **ga** – galea; **gams** – galea mesal seta; **gl** – glossa; **glam** – anterior glossal margin; **glds** – dorsal glossal sclerite; **hysc** – hypostoma carina; **lc** – lacinia; **md** – mandible; **mds** – mandibular sensilla trichodea; **pgb** – postgenal bridge; **plb** – palpus labialis; **pmd** – premental ditch; **pml** – premental lateral surface; **pmv** – ventral premental face; **pmx** – palpus maxillaris; **psm** – postmentum; **st** – stipes; **stg** – stipital groove; **svo** – salivary gland opening. **Symbols**: white arrowhead – depression of the mesal stipital margin receiving the labial palp in retracted position.

of the galea bears a typical maxillary comb (mxc, Fig. 12E). The medial edge of the lacinia bears a row of thin, hair-like spines without articulation (Figs. 8F; 11E).

Musculature (Figs. 9A, B; 11B; 12A).

M. craniocardinalis externus (M. 15 / Omx1): flat and triangular; O: on the ventral posterior head capsule and the posterior half of the postgenal ridge; I: long thin tendon inserted laterally on the proximal end of the cardo. **M. tentoriocardinalis (M. 17 / Omx3) or M. tentoriostipitalis posterior (Omx5):** O: anteriorly on the anterior tentorial arm; I: with a long, thin tendon to an internal process of the stipital base as part of the cardinostipital hinge. **M. tentoriostipitalis (M.18) / M. tentoriostipitalis anterior (Omx4):** two bundles, the anterior one very weakly developed (not tightly attached to the tentorial lamella in one individual) (Fig. 9A, B); O: posterior bundle on the anterior tentorial arm posterad the oblique mesal tentorial lamella, with a few fibers also on the lamella; anterior bundle anteriorly on the ventral side of the mesal lamella (deformed in Fig. 9, but normal in Fig. 11); I: both bundles on long and thin tendons inserted on the internal stipital sclerite, clearly separated from each other, the posterior bundle further proximad. **M. stipitolacinalis (M. 20 / Omx6):** flat muscle; O: laterally on the external stipital sclerite; I: basal lacinial sclerite. **M. stipitogalealis (M. 21 / Omx7):** O: mesally on the external stipital sclerite; I: on a short tendon on the basal galeal sclerite. **M. stipitopalpalis externus (M. 22 / Omx8):** O: external stipital sclerite directly proximad Omx7; I: on a very thin tendon on the lateral base of palpomere 1. **M. palpopalpalis maxillae primus (M. 24 / Omx12):** only the proximal intrinsic palp muscle is recognizable; O: laterally on palpomere 1; I: dorsolateral base of palpomere 2.

Labium and distal hypopharynx: The labium and distal hypopharynx are similar to the homologous structures in other ant species in their general configuration (Figs. 8; 9E - G). The postmentum is thin and horseshoe-shaped (psm, Figs. 8; 9E - G). The only visible premental part in the retracted position is the thin and elongated drop-shaped ventral face (pmv, Figs. 8G; 9F, G); it is surrounded by distinct premental ditches (pmd, Figs. 8G; 9F), which separate it from the extensive lateral face (pml, Figs. 8; 9F, G); the lateral premental surface is entirely covered by the broad external stipital sclerites in their resting position (Fig. 2B); the ventral surface is slightly rugose, whereas the lateral side is glabrous; the well-developed premental arms (pma, Fig. 9G) connect to the thin hypopharyngeal rods (hyr, Fig. 12A), which are anteriorly continuous with the massive distal hypopharyngeal sclerite, the fused hypopharyngeal buttons (hyb, Fig. 12B); the lateral walls of the distal hypopharynx bear dense fringes of minute microtrichia on the dorsal side (dhy, Fig. 8H); the tip of the distal hypopharynx bears defined cell like structures, some of them bearing a single microtrichium (Fig. 8H); the anterodorsal surface is smooth, but a scale-like surface pattern with microtrichia is present posteriorly, towards the infrabuccal pouch (Fig. 12C). The

infrabuccal pouch appears relatively small on longitudinal sections, although a few wrinkles in its wall indicate that it is not fully inflated in the sectioned specimen; the pouch of the μ -CT-scanned individuals is completely wrinkled and mostly empty (ibp, Figs. 10D; 12A, C). The glossa on the dorsal side of the distal labial surface appears diamond-shaped, with the lateral corners rounded in frontal view (gl, Fig. 8A, D, E, G); its posterior / dorsal side is stabilized by the dorsal glossal sclerites (glds, Fig. 8A, E), which form a smooth plate-like structure; ventrally it is stabilized by the rod-like ventral sclerite (glvs, Fig. 12B); the anterior glossal surface is covered with rows of closely set rectangular microtrichia (Figs. 8D; 12E), whereas the microtrichia on the dorsal and ventral margins of the glossa are tapering distally (Fig. 8E). The basiparaglossal brushes proximolaterad the glossa consist of thick, blunt setae (bpb, Figs. 8A; 9G; 11E), increasing in length medially; the bases of the brushes are anteriorly connected to the well-developed, short rod-like paraglossal sclerites; the actual paraglossae are small folds around the sclerites. The two-segmented labial palp is inserted on the distal prementum laterad the paraglossal folds (plb, Fig. 8A, G); the very small palpomere 1 is enclosed by the distal groove on the medial area of the external stipital sclerite and the lateral margin of the distal premental part; the much larger and club-shaped palpomere 2 bears few long thin setae on its distal half and one short and thick seta at its apex.

Musculature (Figs. 9C, D; 11C; 12B).

M. tentoriopraementalis (M. 29 / O1a5): O: posterior head capsule ventrolaterad the occipital foramen; I: the two tendons of the paired muscle merge into a single broad one inserted on the posterior premental margin. **M. praementoparaglossalis (M. 31 / O1a11):** O: laterally on the proximal third of the prementum; I: directly on the base of the ventral glossal sclerite. **M. praementoglossalis (M. 32 / O1a12):** O: on the prementum mesad O1a11; I: base of the dorsal glossal sclerites (Fig. 12B). **M. praementopalpalis externus (M. 34 / O1a14):** O: anteriorly on base of the premental arm; I: base of palpomere 1. **M. palpopalpalis labii primus (M. 35 O1a16):** No intrinsic palp muscles were recognizable. **M. tentoriohypopharyngalis (M42 / Ohy3):** mostly cylindrical but distinctly flattened above the hypostomal cavity when the labium is extended; O: posterior head capsule dorsolaterad O1a5; I: short tendons on the hypopharyngeal buttons close to the salivarium.

Salivarium and salivary duct: The slender salivary duct is lined by a thin layer of cuticle (svd, Figs. 9C, D; 11C). It forms a dorsally oriented loop directly posterad the infrabuccal pouch when the maxillolabial complex is in its retracted position, but straightens out when the complex is extended (Fig. 11C). The duct is distally inserted on the sclerotized salivarium (sv, Figs. 10D; 11C; 12B); the salivary sclerite is U-shaped and almost vertically oriented in its resting position; the salivary opening is located between the basiparaglossal brushes behind the glossa and flanked by a few microtrichia (svo, Fig. 8I).

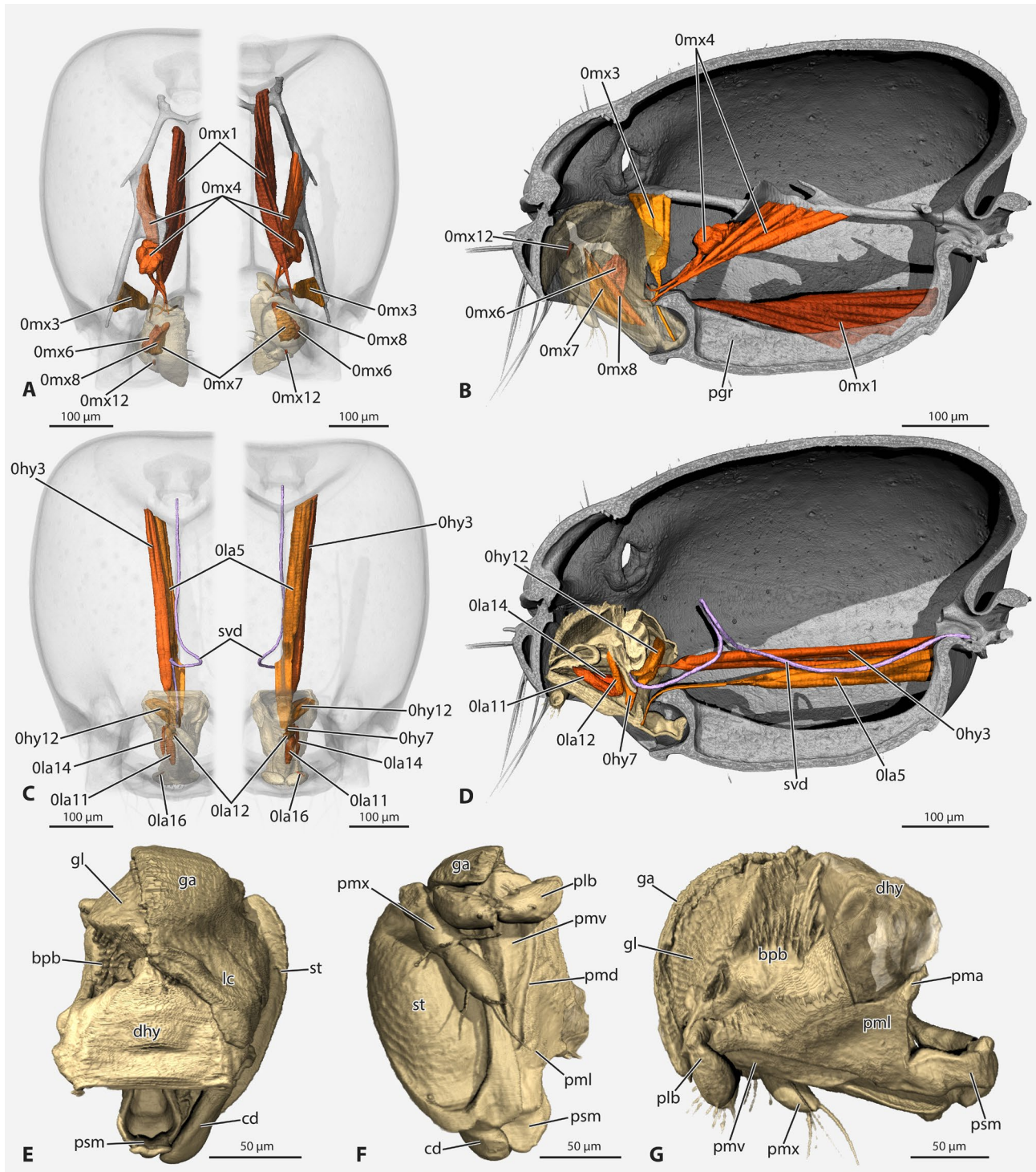


Fig. 9: Volume renderings of heads of *Protanilla lini* (CTAR0046). **A, C**: Left part dorsal, right part ventral view. **B, D**: Sagittal view. **E**: Dorsal view. **F**: Ventral view. **G**: Lateral view. **A, B**: Maxillary musculature. **C - D**: Labial musculature and salivary duct. **E - G**: Isolated labium (with distal hypopharynx) and right maxilla. **Abbreviations**: **0hy3** – M. tentoriohypopharyngalis; **0hy7** – M. praementosalivarialis; **0hy12** – M. hypopharyngosalivarialis; **0la5** – M. tentoriopraementalis; **0la11** – M. praementoparaglossalis; **0la12** – M. praementoglossalis; **0la14** – M. praementopalpalis externus; **0la16** – M. palpopalpalis labii primus; **0mx1** – M. craniocardinalis externus; **0mx3** – M. tentoriocardinalis; **0mx4** – M. tentoriostipitalis anterior; **0mx6** – M. stipitolacinalis; **0mx7** – M. stipitogalealis; **0mx8** – M. stipitopalpalis externus; **0mx12** – M. palpopalpalis maxillae primus; **cd** – cardo; **bpb** – basiparaglossal brush; **dhy** – distal hypopharynx; **ga** – galea; **gl** – glossa; **lc** – lacinia; **pgr** – postgenal ridge; **plb** – palpus labialis; **pma** – premental arm; **pmd** – premental ditch; **pml** – premental lateral surface; **pmv** – ventral premental face; **pmx** – palpus maxillaris; **psm** – postmentum; **st** – stipes; **svd** – salivary duct. **Colors**: beige / brown – mouthparts; grey – cuticle; orange / red – muscles; purple – gland duct.

Musculature (Figs. 9C, D; 11C; 12B). **M. hypopharyngosalivariialis (M. 37 / Ohy12):** two closely adjacent bundles; O: dorsolaterally on the hypopharyngeal rod; I: one pair of bundles dorsally on the distal salivary duct, the other one laterally on the proximal end of the U-shaped salivary sclerite. **M. praementosalivariialis anterior & (or) posterior (M. 38, 39 / Ohy7):** very indistinct, only one or two fibers; O: proximally on the prementum, proximad 0la12; I: ventrally on the salivary sclerite.

Distal epipharynx: The distal epipharynx forms the upper wall of the laterally open buccal cavity (ep, Figs. 10A, D; 11A; 12A). Its main dome-shaped part is laterally delimited by longitudinal folds when the mouthparts are retracted; the epipharynx appears more lobe-like with several wide longitudinal folds when the mouthparts are in their extended position (Fig. 11A). The surface is largely smooth, without fringes of longer microtrichia; long microtrichia are restricted to the area of the upper lip of the functional mouth opening, at the anterior margin of the dorsal prepharyngeal wall.

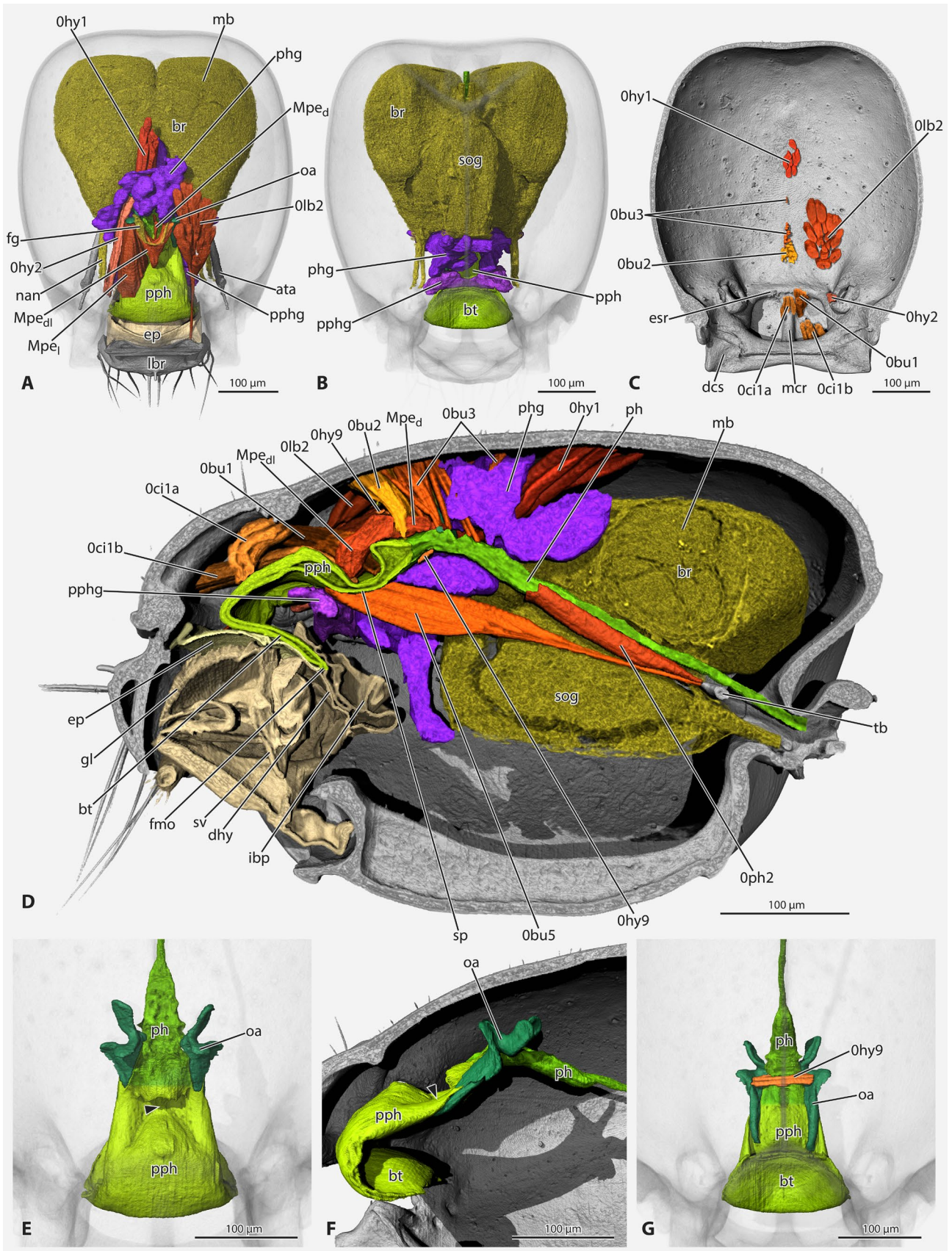
Musculature. Epipharyngeal muscles function as part of the cephalic digestive tract and are treated in that section.

Cephalic digestive tract: The general configuration of the formicid cephalic digestive tract is maintained, with a prepharynx formed by lateral fusion of the proximal epi- and hypopharynx (pph, Figs. 10; 11A; 12A). The prepharynx is distinctly bent backward when the mouthparts are in a retracted position, thus forming the buccal tube (bt, Fig. 10); this angle of about 60° is straightened out when the mouthparts are extended, with the whole anterior part of the prepharynx evenly and gradually sloping downwards (Figs. 11A; 12A); a deep transverse indentation of the dorsal prepharyngeal wall shortly anterad the anatomical mouth opening is less distinct when the mouthparts are extended. The cuticle is very thin (ca. 1 µm) in this area; in contrast, the dorsal prepharyngeal (epipharyngeal) wall is very thick (ca. 6-7 µm) anterior to the indentation, but continuously thins out towards the functional mouth opening (ca. 2 µm); the thickness of the ventral (hypopharyngeal) cuticle of the prepharynx, which forms the sitophore plate (sp, Figs. 10D; 12A), is more uniform (ca. 2-3 µm); only the distal region of the dorsal prepharyngeal wall bears distinct microtrichia (up to ca. 3.5 µm, Fig. 12C), whereas only minute ones (< 1 µm) are

present on the remaining surface up to the level of muscle Oci1a (Fig. 12D); a sparse vestiture of microtrichia (up to ca. 3.5 µm close to the functional mouth opening) on the ventral prepharyngeal (hypopharyngeal) surface reaches the same level (Fig. 12D); all hairs are inclined towards the functional mouth opening (fmo, Fig. 10D); the prepharynx is stabilized by the intricately shaped sclerotized oral arms (oa, Fig. 10E - G), which originate as small stumps on the ventral wall of the anterior prepharynx; they increase in length posteriorly and shift laterally on the prepharynx; on the level of the anatomical mouth opening, the arms are bent upwards at an angle of almost 90° and form a vertical plate; behind the plate, the arms form free, posteriorly directed and apically rounded processes. The pharynx following the anatomical mouth opening (marked by the frontal ganglion and muscles Obu2 and Ohy1) has a very narrow lumen and is approximately round in cross section, but with flat irregular longitudinal folds (ph, Figs. 10; 11A); it is slightly bent downwards at an angle of about 50° shortly posterad the anatomical mouth opening.

Musculature (Figs. 10; 11A). **M. frontohypopharyngealis / M. frontooralis (M. 41 / Ohy1):** a long muscle (Fig. 10A); O: posterior frontal region close to the midline, far posterad the other frontal muscles (Fig. 10C). I: posterior side of the posterior process of the oral arms. **M. clypeopalatalis (M. 43 / Oci1):** an unpaired (a) and paired (b) subcomponent; Oci1a: O: anteriorly on the epistomal ridge (Fig. 10C); I: dorsal prepharyngeal wall, half distance between the indentation and the bend of the buccal tube (Fig. 12D); curved in an irregular manner in the specimen scanned with the mouthparts in retracted position (Fig. 10D), but straight in the individuals with extended mouthparts (µ-CT scan and sections, Fig. 11A). Oci1b: O: anterolaterally on the clypeus (Fig. 10C); I: on the thickest part of the dorsal prepharyngeal wall (Fig. 10D). **M. clypeobuccalis (M. 44 / Obu1):** O: on the clypeus directly anterad the epistomal ridge, laterad the mid-clypeal ridge (Fig. 10C); I: dorsal prepharyngeal wall in the area of the indentation (Fig. 10D). **M. frontobuccalis anterior (M. 45 / Obu2):** unpaired muscle; O: anterior frontal region on the level of the frontal ganglion (Fig. 10C); I: dorsal wall of the pharynx at the anatomical mouth opening directly posterad the frontal ganglion (Fig. 10D). **M. frontobuccalis posterior (M. 46 / Obu3):** unpaired, rather loose fibers; O: frontal region directly posterad Obu2, one isolated fiber slightly further

Fig. 10: Volume renderings of heads of *Protanilla lini* (CTAR0046). **A, E:** Dorsal view. **B, C, G:** Ventral view. **D, F:** sagittal view. **A, B, D:** Cephalic digestive tract with its musculature, glands, and the central nervous system. **C:** Origin sites of the dorsal muscles of the cephalic digestive system. **D, E:** Prepharynx with oral arms. **Abbreviations:** **Obu1** – *M. clypeobuccalis*; **Obu2** – *M. frontobuccalis anterior*; **Obu3** – *M. frontobuccalis posterior*; **Obu5** – *M. tentoriobuccalis posterior*; **Oci1a** – *M. clypeopalatalis*, unpaired portion; **Oci1b** – *M. clypeopalatalis*, paired portion; **Ohy1** – *M. frontooralis*; **Ohy2** – *M. tentoriooralis*; **Ohy9** – *M. oralis transversalis*; **Olb2** – *M. frontoepipharyngalis*; **Oph2** – *M. tentoriopharyngalis*; **ata** – anterior tentorial arm; **br** – brain; **bt** – buccal tube; **dcs** – distal ventral clypeal surface; **dhy** – distal hypopharynx; **ep** – epipharynx; **esr** – epistomal ridge; **fg** – frontal ganglion; **fmo** – functional mouth opening; **gl** – glossa; **ibp** – infrabuccal pouch; **lbr** – labrum; **mb** – mushroom bodies; **mcr** – medial clypeal ridge; **Mpe_d** – *M. pharyngoepipharyngalis*, dorsal portion; **Mpe_{dl}** – *M. pharyngoepipharyngalis*, lateral dorsal portion; **Mpe_l** – *M. pharyngoepipharyngalis*, lateral portion; **nan** – antennal nerve; **oa** – oral arm; **ph** – pharynx;



phg – pharyngeal gland; **pph** – prepharynx; **pphg** – prepharyngeal gland; **sog** – suboesophageal ganglion; **sp** – sitophore plate; **sv** – salivarium; **tb** – tentorial bridge. **Colors:** beige / brown – mouthparts; dark green – oral arms; green – cephalic digestive tract (prepharynx and pharynx); grey – cuticle; orange / red – muscles; purple – glands; yellow – nervous system. **Symbols:** black arrowhead – dorsal groove of the prepharynx.

posterad; (Fig. 10C) I: directly posterad Obu2 (Fig. 10D). **M. frontobuccalis lateralis / M. tentoriooralis (M. 47 / Ohy2)**: a long, flat muscle (Fig. 10A); O: internally on the anterior thickened part of the torulus (Fig. 10C); I: anteriorly on the apex of the posterior process of the oral arm. **M. tentoriobuccalis anterior (M. 48 / Obu5) (possibly together with M.50 / Obu6)**: a well-developed unpaired muscle (Fig. 10C); O: on a long, thin tendon on the anterior process of the tentorial bridge; I: broadly on the ventral prepharyngeal wall (sitophore plate) around the level of the indentation of the dorsal wall. **M. tentoriopharyngalis (M. 52 / Oph2)**: a relatively long and thin muscle (Fig. 10C); O: on the tentorial bridge laterad Obu5; I: on the ventral and lateral pharynx, closer to the anatomical mouth opening than to the tentorial bridge. **M. transversalis buccae (M. 67) / M. oralis transversalis (Ohy9)**: a well-developed muscle with a dorsal and ventral portion; the dorsal portion connects the vertical plates of the oral arms on the dorsal side and is curved anterad around Obu2 together with the frontal ganglion (Fig. 10A); the ventral portion connects the vertical plates of the oral arms ventrally in a straight line (Fig. 10G). **M. annularis stomadaei (M. 68 / Ost1)**: a thin layer of ring muscles around the pharynx. **M. longitudinalis stomadaei (M. 69 / Ost2)**: a thin layer of longitudinal muscles below the ring muscle layer. **M. pharyngoepipharyngealis (Mpe)**: very strongly developed longitudinal muscles connecting the anterior pharynx and the dorsal prepharyngeal wall (Fig. 10A); a very thin unpaired mesal bundle connects the pharyngeal wall at the level of Obu3 with the thickened prepharyngeal wall at the level of Oci1b; two thicker bundles originate mesally on the dorsal portion of the oral arms, converge mesally, and insert together with the unpaired mesal bundle; the two largest bundles originate anteriorly on the vertical plates of the oral arms and insert broadly on the lateral area of the prepharyngeal (epipharyngeal) wall with thickened cuticle.

Cephalic glands: The voluminous mandibular gland is a cluster of eight to nine large cells, located laterally in the middle region of the head, of irregular shape, and with a diameter of up to about 40 µm; the complex of cells is attached to a large, flat reservoir extending beyond the cell cluster along most of the lateral wall of the head capsule (mdg, Fig. 6C, D); anteriorly this cavity narrows and forms a cylinder; its proximal section is rather thick, but it narrows strongly when it enters the basal mandibular tunnel; in cross section, this distal section appears T- or anchor-shaped together with a stabilizing membrane (Fig. 4C); finally, the duct opens on the membranous field of the mandalus. A glandular epithelium is present on

the inner mandibular wall around the lateral proximal base (mdig, Fig. 12F), characterized by larger cells with larger nuclei compared with other epithelial tissue in the mandible. A distinct maxillary gland is lacking, but gland cells are present within the galeolacinal complex (glig, Fig. 12E). The well-developed prepharyngeal gland below the prepharynx is formed by a flat cluster of about 16 gland cells, each with a diameter of about 23 µm (pphg, Fig. 10A, B, D). Additionally, a glandular epithelium is present on the ventral prepharyngeal wall, especially in the region of the buccal tube and also continuing to the infrabuccal pouch (ppheg, Figs. 11A; 12A, C, D). The pharyngeal gland, the largest of the head, is glove-shaped like in many other ants, but the tubular extensions are short and all of them irregularly shaped (possibly partly due to insufficient tissue preservation); they open into the pharynx at the level of the posterior oral arms (phg, Fig. 10A, B, D).

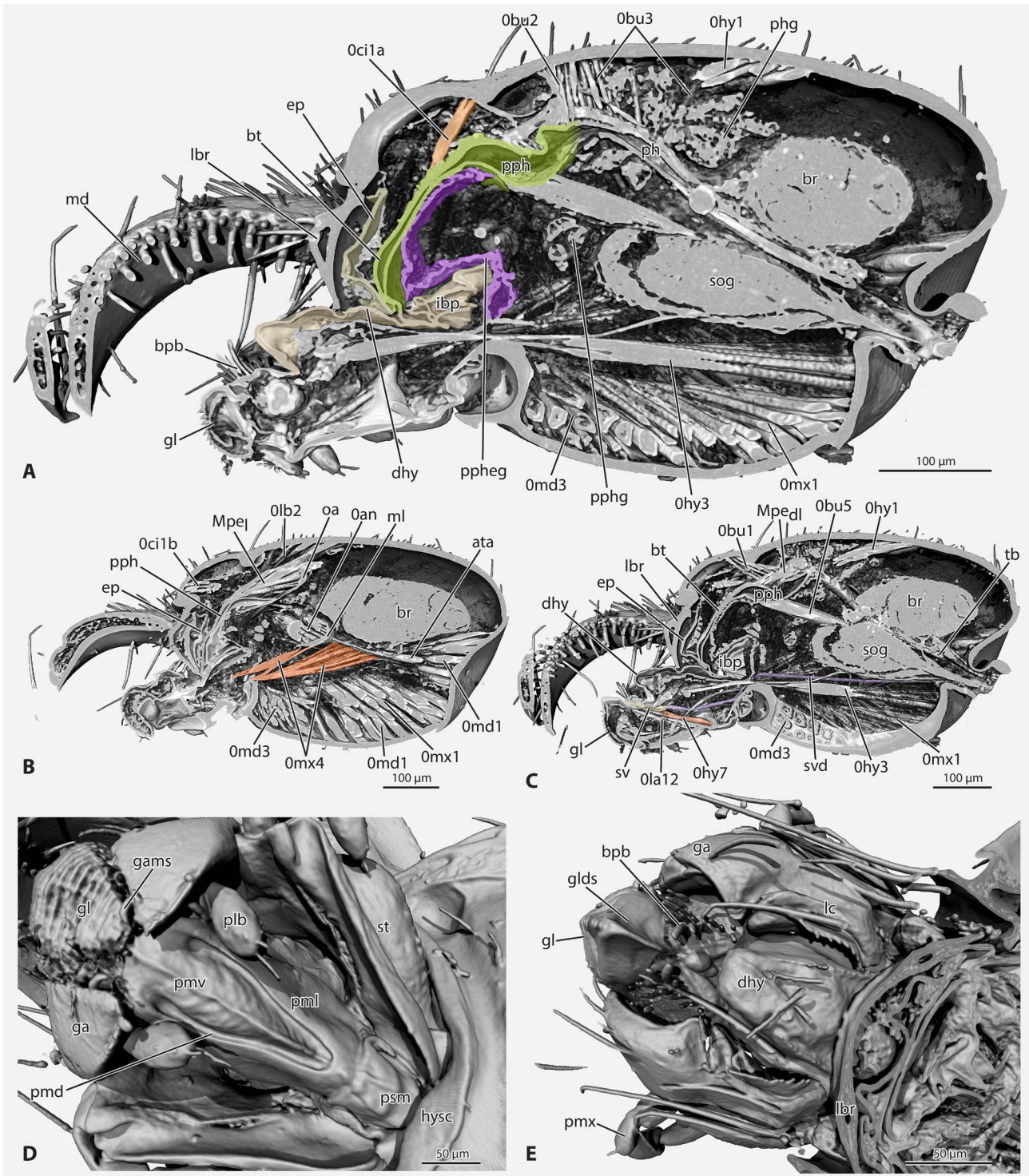
Brain and suboesophageal complex: The brain fills out a large portion of the cephalic lumen (br, Figs. 10A, B, D; 11A - C). As in other ants, the brain and suboesophageal ganglion (sog, Figs. 10A, B, D; 11A - C) form a very compact unit, with a thin passage between them for the pharynx and muscles Obu5 and Oph2. The brain is distinctly broader posteriorly and narrows anteriorly; it is emarginated dorsally between the bulging antennal lobes, and a smaller indentation is present posteriorly. Optic neuropils are completely absent. The mushroom bodies (mb, Fig. 10A, D) are large in cross section, resulting in the increased width of the posterior protocerebrum, despite of the absence of the optic lobes. The antennal nerves split shortly after their origin on the deutocerebral antennal lobes and extend into the scapus and antennal flagellum (nan, Fig. 10A, B); frontal commissures originating mesad the antennal lobes have a slightly oblique anterior orientation; the frontal ganglion is very narrow and curved around muscle Obu2 anteriorly (fg, Fig. 10A). The suboesophageal complex is almost as long as the brain, but only about one third as broad; it is connected to the prothoracic ganglion by two closely adjacent connectives, with a rather short section within the head, due to the position of the occipital foramen.

Fat body: Fat body cells are loosely arranged around all other organs; they are concentrated close to the inner clypeal wall and in the lumen of the labrum and mandibles.

Discussion

Mandible movements in *Protanilla*: A hypothetical pattern of movements of the mandibles of *Protanilla* species (*Protanilla lini* and *Protanilla rafflesi*) is outlined in the following section, based on morphological observations, manipulation of the printed model, and animations.

Fig. 11: Volume renderings of heads of *Protanilla lini* (CTAR0047), unsegmented renders with selected structures marked in photoshop. **A - C:** Sagittal view, **A:** central section, **B:** lateral section, **C:** lateral section, close to central. **D:** Ventral view. **E:** Dorsal view. **A:** Anterior cephalic digestive tract marked. **B:** Omx4 marked. **E:** Maxillolabial complex. **Abbreviations:** **Oan** – antennal musculature; **Obu1** – M. clypeobuccalis; **Obu2** – M. frontobuccalis anterior; **Obu3** – M. frontobuccalis posterior; **Obu5** – M. tentoriobuccalis posterior; **Oci1a** – M. clypeopalatalis, unpaired portion; **Oci1b** – M. clypeopalatalis, paired portion;



0hy1 – M. frontooralis; **0hy3** – M. tentoriohypopharyngalis; **0hy7** – M. praementosalivarialis; **0la12** – M. praementoglossalis; **0lb2** – M. frontoepipharyngalis; **0md1** – M. craniomandibularis internus; **0md3** – M. craniomandibularis externus; **0mx1** – M. craniocardinalis externus; **0mx4** – M. tentoriostipitalis anterior; **ata** – anterior tentorial arm; **bpb** – basiparaglossal brush; **br** – brain; **bt** – buccal tube; **dhy** – distal hypopharynx; **ep** – epipharynx; **ga** – galea; **gams** – galea mesal seta; **gl** – glossa; **glds** – dorsal glossal sclerite; **hysc** – hypostoma carina; **ibp** – infrabuccal pouch; **lbr** – labrum; **lc** – lacinia; **md** – mandible; **ml** – mesal tentorial lamella; **Mpe_l** – M. pharyngoepipharyngalis, lateral dorsal portion; **Mpe_d** – M. pharyngoepipharyngalis, lateral portion; **oa** – oral arm; **ph** – pharynx; **phg** – pharyngeal gland; **plb** – palpus labialis; **pmd** – premental ditch; **pml** – premental lateral surface; **pmv** – ventral premental face; **pmx** – palpus maxillaris; **psm** – postmentum; **pph** – prepharynx; **ppheg** – prepharyngeal epithelial gland; **pphg** – prepharyngeal gland; **sog** – suboesophageal ganglion; **st** – stipes; **svd** – salivary duct; **sv** – salivarium; **tb** – tentorial bridge. **Colors: beige / brown** – distal epi- and hypopharynx (not part of prepharynx); **green** – prepharynx; **grey** – cuticle and not marked internal tissue; **orange** – muscles; **purple** – glands.

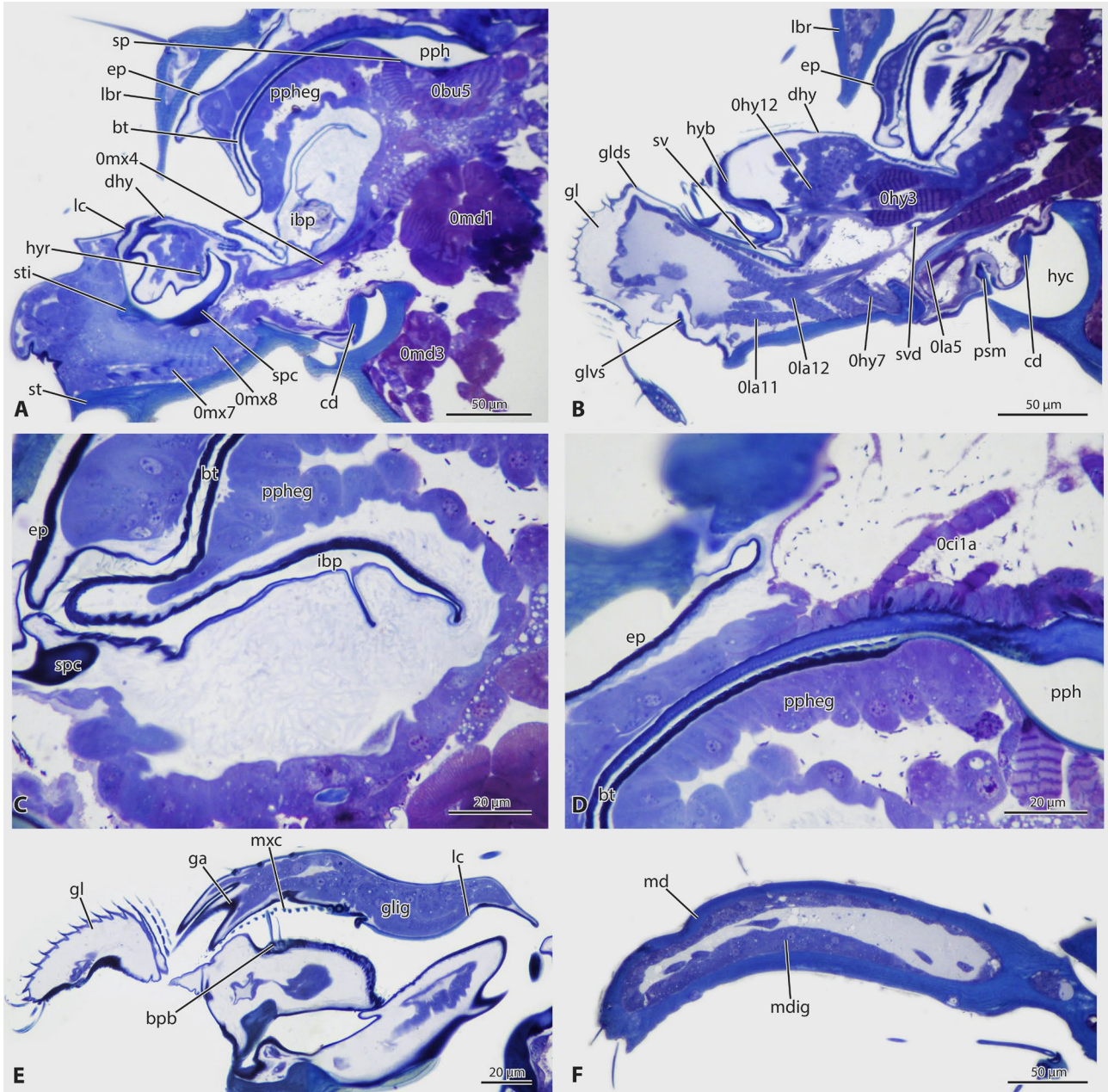


Fig. 12: Histological sections of heads of *Protanilla lini*. All sections longitudinal with anterior to the left. **A:** Anterior head at stipital level. **B:** Parasagittal section through labium. **C:** Detail of the functional mouth and infrabuccal pouch. **D:** Detail of the insertion site of *Oci1a*. **E:** Section through the galeolacinal complex with internal gland tissue. **F:** Section through the mandible with internal gland tissue. **Abbreviations:** **Obu5** – M. tentoriobuccalis posterior; **Oci1a** – M. clypeopalatalis, unpaired portion; **Ohy3** – M. tentoriohypopharyngalis; **Ohy7** – M. praementosalivarialis; **Ohy12** – M. hypopharyngosalivarialis; **Ola5** – M. tentoriopraementalis; **Ola11** – M. praementoparaglossalis; **Ola12** – M. praementoglossalis; **Omd1** – M. craniomandibularis internus; **Omd3** – M. craniomandibularis externus; **Omx4** – M. tentoriostipitalis anterior; **Omx7** – M. stipitogalealis; **Omx8** – M. stipitopalpalis externus; **bpb** – basiparaglossal brush; **bt** – buccal tube; **cd** – cardo; **dhy** – distal hypopharynx; **ep** – epipharynx; **ga** – galea; **gl** – glossa; **glds** – dorsal glossal sclerite; **glig** – galeolacinal complex gland; **glvs** – ventral glossal sclerite; **hyb** – hypopharyngeal button; **hyc** – hypostomal cavity; **hyr** – hypopharyngeal rod; **ibp** – infrabuccal pouch; **lbr** – labrum; **lc** – lacinia; **md** – mandible; **mdig** – mandible internal gland; **mx** – maxillary comb; **sp** – sitophore plate; **pph** – prepharynx; **ppheg** – prepharyngeal epithelial gland; **psm** – postmentum; **svd** – salivary duct; **spc** – stipito-premental conjunctivum; **st** – stipes; **sti** – stipes internal sclerite; **sv** – salivarium.

The mandibles of pterygote dicondylic insects (except for mayflies and forms with reduced or modified mandibles) are articulated with the head capsule at two

defined points, (1) the primary mandibular joint with a mandibular condyle and a cephalic acetabulum, and (2) the secondary joint with a mandibular acetabulum and a

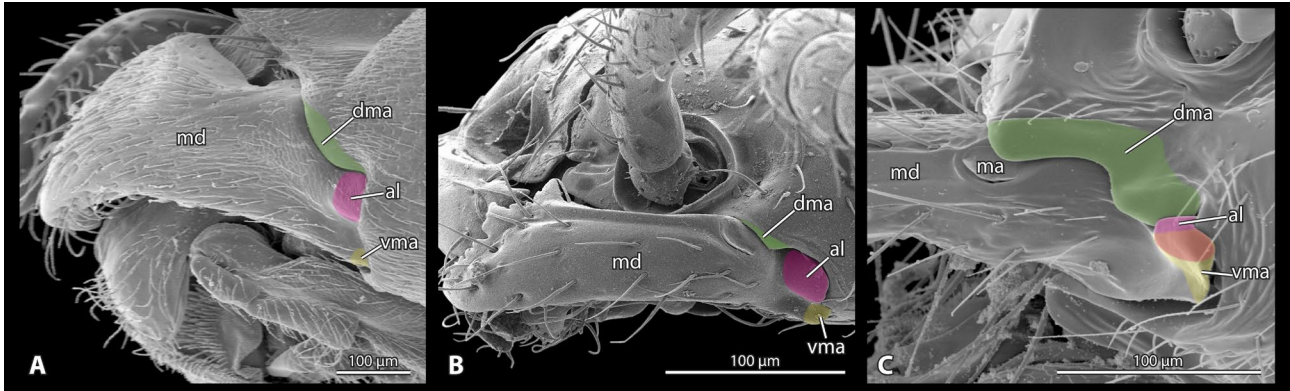


Fig. 13: Scanning Electron Microscopy micrographs of the mandibular articulation of *Formica rufa* (A), *Leptanilla swani* (B), and *Protanilla lini* (C), all in lateral view. The dorsal (secondary) clypeal condyle of the mandibular articulation is shaped very similarly in *Formica* and *Leptanilla* but highly modified in *Protanilla*. The atala is far separated from the ventral (primary) mandibular condyle in *Formica* while they are very close and almost set in the same cephalic acetabulum in *Leptanilla*. In *Protanilla*, they are completely fused. Clypeal condyle colored in green, atala in red, and mandibular condyle in yellow. In *Protanilla*, the marking of atala and mandibular condyle are shown as overlapping; it is not clear if the single articulatory process represents the atala with strong reduction of the ventral articulation, or if the division between the two parts is marked by the groove in the fused articulatory process. **Abbreviations:** al – atala; dma – clypeal condyle; ma – mandalus; md – mandible; vma – mandibular condyle.

cephalic condyle. As both articulations are usually developed as “ball and socket joints”, this type of articulation restricts the movement of the mandible to a single plane and allows for a more forceful bite (BEUTEL & al. 2014).

In ants, the secondary (dorsal) joint (dma, Fig. 13A, B) is enlarged dorsoventrally (RICHTER & al. 2019, 2020), which likely increases the degree of freedom for mandibular opening, and may explain the broader gape and biaxial rotation via a cam-lock mechanism as previously observed (GRONENBERG & al. 1998, ZHANG & al. 2020). However, the specific functional consequences of this modified articulation have yet to be studied in detail. Ant mandibles are further characterized by the presence of the atala (al, Fig. 13A, B; “abductor swelling”, MICHENER & FRASER 1978), a lateral process set in a cephalic acetabulum that serves as a lever arm for the mandibular abductor (*M. craniomandibularis externus*, 0md3).

In *Protanilla* (*Protanilla lini* and *Protanilla rafflesii*), the mandibular articulation is modified and differs distinctly from this general ant pattern. The anterior margin of the clypeus projects anteriorly, and the secondary (dorsal) condyle is extended anterad along with it (dma, Fig. 13 C). This forms the distal clypeal knob, which creates an additional point of articulation. As a second important modification, the atala is fused with the primary (ventral) condyle of the mandible to form a single ventrolateral articulatory process. This structural modification of the mandibular articulation is worth noting in the context of field observations of *Protanilla*, where they have been seen opening their mandibles at an angle of about 180° and rapidly snapping shut (HÖLLDOBLER & WILSON 1990, HSU & al. 2017). Additionally, two low framerate videos by Mark K. L. Wong document this behavior (Videos S4, S5). While there is currently no direct evidence for a

power-amplified mechanism as it is observed for trap-jaw ants (reviewed by LARABEE & SUAREZ 2014), we present a hypothesis on how the mandible of *Protanilla* moves and how a potential trap-jaw mechanism could function. In this context, it should be clearly stated that, currently, no reliable measurements are available to show that the mandibles of *Protanilla* close particularly faster than those of “normal” or “generalized” ant species (see GRONENBERG & al. 1997). The framerate of available videos (Videos S4, S5) is not sufficient to confirm this. To prove the presence of a power amplification, it would be necessary to show that mandibles move faster than would be possible based on muscular contraction alone (LARABEE & SUAREZ 2014). Testing this hypothesis would require living specimens and quantification of the rate of mandibular closure via high-speed filming, as in studies on “true” trap-jaw ants (GRONENBERG 1995, 1996, PATEK & al. 2006, LARABEE & al. 2017, WANG & al. 2020).

When the mandibles are closed, the groove on the ventral articulatory process locks with the corresponding hump in the cephalic acetabulum (Fig. 14B), supported by the interactions with the labral grooves and hypostomal process. In our experiments with 3D prints (Video S5), this very effectively locks the mandibles in place. Together with the strong mandibular traction chaetae, this probably allows for tight grasp of the prey. To initiate the release of the locked state, the conspicuous protrusion of the process must first be unlocked in a slight downwards motion, indicated by the visible gap between process and acetabulum in resting position (Fig. 2C). This motion is enabled by the oblique downwards orientation of the mandibular abductor apodeme and its muscle (*M. craniomandibularis externus*, 0md3). The initial opening rotation is dorsally stabilized by the distal clypeal knob and the corresponding

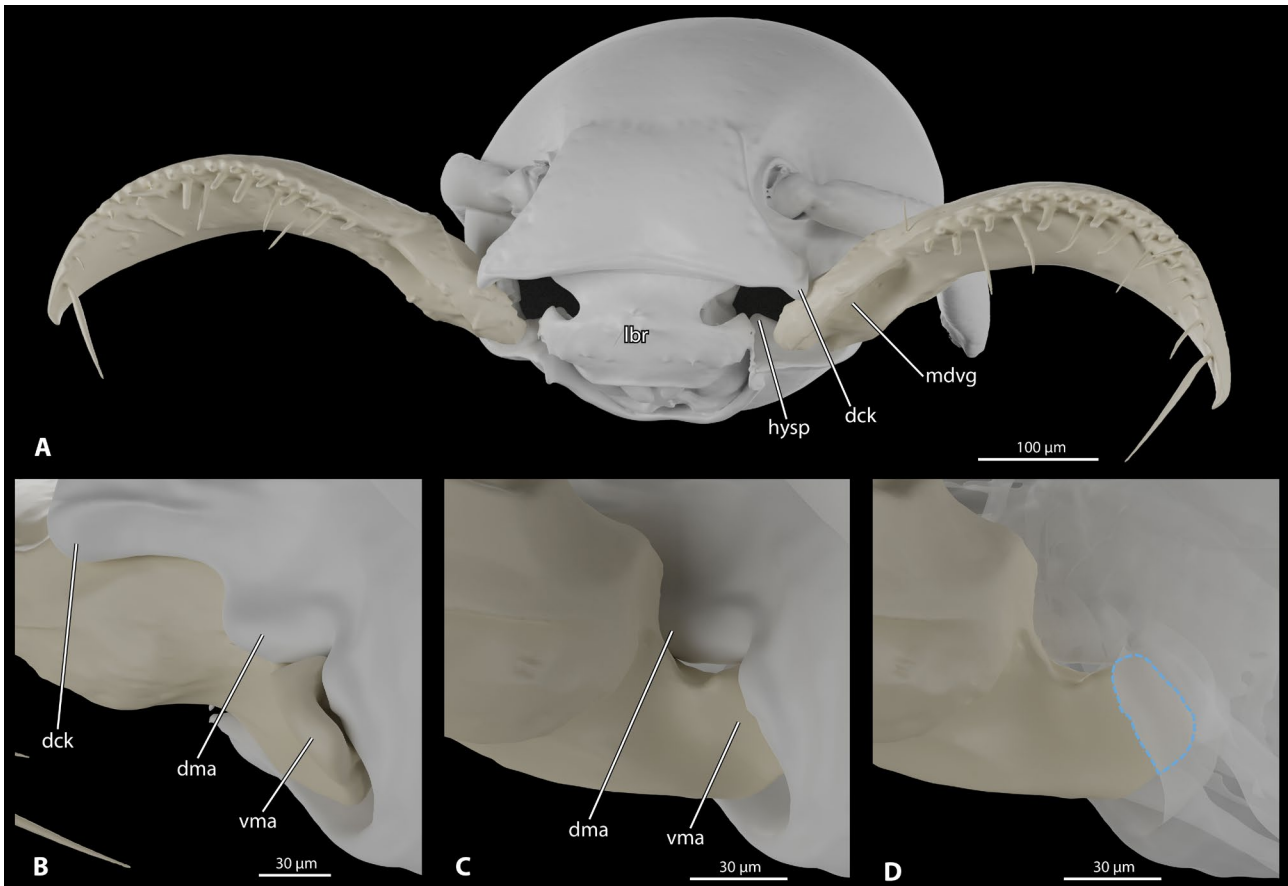


Fig. 14: Surface renderings of the head of *Protanilla lini* (A) with open mandibles, frontolateral view. (B) Mandibular articulation with mandible closed, lateral view. (C) Mandibular articulation with mandible open, lateral view. (D) Mandibular articulation with mandible open, structures transparent to show position of ventral mandibular condyle, lateral view. **Abbreviations:** **dck** – distal clypeal knob; **dma** – clypeal condyle; **hysp** – hypostoma triangular process; **mdvg** – mandible ventral groove; **vma** – mandibular condyle cuticle. **Symbols:** blue outline – portion of the ventral mandibular condyle locked in the notch of the acetabulum.

furrow on the mandible (Video S2). Ventrally, the labral grooves and the hypostomal triangular process interact with the medial mandibular margin and the deep ventral groove of the mandible. To reach the fully open position of about 180°, the articular process traverses the hump of the acetabulum and finally slips conspicuously into the notch between condyle and acetabulum hump (Fig. 14C, D; Video S2). In the fully opened position, the auxiliary guide rails (clypeal knob, labral groove, hypostomal process) lose contact with their corresponding mandibular surfaces, which indicates that the final rotation and locking into the notch may be similar to cocking a crossbow. Potentially, the clypeal knob can serve to keep the medial margin of the mandible in this position. So far, it is unclear if the process resting in the notch is suited to build up sufficient energy to qualify as a power-amplification thus trap-jaw mechanism (LARABEE & SUAREZ 2014). However, the elongated setae on the mandibular apex and the labrum could potentially serve as trigger hairs, which supports the presence of at least a trap-jaw-like mechanism. While in several myrmicine genera with trap-jaws the labrum plays a role in locking the mandible in position to generate power, this is clearly not the case in *Protanilla*, despite the peculiar

shape of the labrum. Our results do not support any direct interactions of the mandible with the labrum apart from the “guide rail” function of the labral grooves (Video S1). Videos of the mandible movement in vivo also show that the mandibles can be snapped closed independently (Videos S4, S5), providing further evidence against the labrum as locking mechanism. In any case, the mandible seems to close rapidly, and we infer that this movement is stabilized by regaining contact with the dorsal and ventral guide rails. It is conceivable that these compensate for higher flexibility, which is due to the loose main articulation.

On the one hand, the modified mandibular articulation of *Protanilla* possibly enables the advantages of the typical dicondylic articulation, that is, restricted but forceful biting movement and easy control with only two muscles (BLANKE 2019). On the other hand, it would possess those of a less restricted articulation with higher degrees of freedom, that is, finely adjusted mandibular control and movements in different directions, potentially including optimal attack angles for the traction chaetae and a very tight grip. It is also noteworthy in this context that the fibers of the mandibular adductor (Omd1) are attached very steeply on the tendon (on average 23.06°). Although

Tab. 2: Comparison of the musculature of ants with two aculeate outgroups. Muscle numbers follow RICHTER & al. (2020), based on WIPFLER & al. (2011), or the respective reference for the taxon. O: muscle present, ×: muscle absent, ?: muscle not described in the respective study, but possibly omitted rather than confirmed absent, lm: prepharyngeal longitudinal muscles, Mpe: M. pharyngoepipharyngealis.

Family	Vespidae	Crabronidae	Formicidae				
Species	<i>Vespa pensylvanica</i>	<i>Pison chilense</i>	<i>Wasmannia affinis</i>	<i>Neoponera villosa</i>	<i>Protanilla lini</i>	<i>Formica rufa</i>	<i>Brachyponera luteipes</i>
Reference	DUNCAN (1939)	ZIMMERMANN & al. (2016)	RICHTER & al. (2019)	PAUL & al. (2002)	Present study	RICHTER & al. (2020)	
0an1	end	0an1	M1	(18)	○	○	○
0an2	ial	0an2	M2	(17)	○	○	○
0an3	eal	0an3	M3	(18)	○	○	○
0an4	iad	0an4	M4	(17)	○	○	○
0an6	?	?	M5	?	○	○	○
0an7	?	?	M6	?	○	○	○
0lb2	×	0lb 2	M9	(19)	○	○	○
0md1	admd	0md1	M11	mc	○	○	○
0md3	abmd	0md3	M12	mo	○	○	○
0md8	?	0md8	M13	?	○	○	○
0mx1	pcd	0mx1	M15	(11)	○	○	○
0mx3/ 0mx5	exm	0mx3/ 0mx 5	M17	(13)	○	○	○
0mx4	flst	0mx4	M18	(12)	○	○	○
0mx6	flc	0mx6	M20	(15)	○	○	○
0mx7	fga	0mx7	M21	(14)	○	○	○
0mx8	pdmp	0mx8	M22	(16)	○	○	○
0mx10	admp	×	×	×	×	×	×
0mx12	?	?	M24	?	○	○	○
0mx13	?	?	×	?	×	○	×
0la5	plad	0la5	M29	(6)	○	○	○
0la11	pffi	0la11	M31	(8)	○	○	○
0la12	afli	0la12	M32	(9)	○	○	○
0la14	dlbp	0la14	M34	Palpus muscle	○	○	○
0la16	?	?	M35	?	×	○	○
0la17	?	?	×	?	×	○	×
0hy1	?	0hy1	M41 b	(1)	○	○	○
0hy2	lphm	0hy1	M41 a	?	○	○	○
0hy3	fgpl	0hy3	M42	(7)	○	○	○
0hy7	×	×	M38	(9)	○	○	○
0hy9	atim, ptim	?	M67	(4)	○	○	○
0hy12	dmslv, pmslv	0hy12a/ b	M37	(10)	○	○	○
0ci1 a	cdmth	0ci1	M43 a	(5)	○	○	○
0ci1 b	dlbc	0bu1	M43 b	(1)	○	○	○
0bu1	dlbc	0bu1	M44	(1)	○	○	○
0bu2	1 dlph	0bu2	M45	(1)	○	○	○
0bu3	?	0bu3	M46	?	○	○	×
0bu5	3 dlph?	0bu5	M48	(1)?	○	○	○
0bu6	3 dlph	0bu6	M50	(1)	○	○	○
0ph1	2 dlph	0ph1	×	×	×	×	×
0ph2	4 dlph	0ph2	M52	(2)	○	○	○
0st1	?	?	M68	?	○	○	○
0st2	dim	?	M69	?	○	○	○
Mpe	pdmth	Mpe	Lm	(3)	○	○	○

this is not in the range of the smallest attachment angles measured in ants, it is arguably in the realm prioritizing faster rather than especially powerful mandibular closing (PAUL & GRONENBERG 1999). In this, the configuration in *Protanilla* appears somewhat similar to that described for non-trap-jaw species of *Strumigenys* F. SMITH, 1860 (former “*Pyramica*”; BOOHER & al. 2021). Together with strongly developed directly attaching muscle fibers with short sarcomeres, this suggests that rather than achieving fast mandibular closure through a power-amplification mechanism, such an effect may be achieved by fast muscle contraction in combination with an elongate mandible, leading to a high angular momentum of the apex relative to the base.

Leptanillomorph mosaicism: Given the strong signal for the placement of Leptanillomorpha (Martialinae, Leptanillinae) as sister to all other crown group ants (poneroformicine clade) (e.g., BRADY & al. 2006, MOREAU & al. 2006, RABELING & al. 2008, KÜCK & al. 2011, MOREAU & al. 2013, WARD 2014, BRANSTETTER & al. 2017, BOROWIEC & al. 2019), we are compelled to ask: Are the Leptanillinae (and Martialinae) mainly characterized by unique apomorphies or do they retain many plesiomorphies relative to their sister group? Ecologically, there is evidence that Leptanillomorpha are derived relative to the estimated crown group life history (LUCKY & al. 2013, NELSON & al. 2018, WONG & GUÉNARD 2020, KELLER & PEETERS 2020), being specialized subterranean predators of Geophilomorpha, perhaps surviving the End Cretaceous crisis due to an unusually stable environment, accessible through a suite of hypogaecic adaptations. Interestingly, we identified only two potential cephalic plesiomorphies retained relative to poneroformicine ants in our evaluation of cephalic structures of *Protanilla lini*. In contrast, we found many presumptive apomorphies shared between the species of Leptanillinae and *Martialis*, apparently related to their hypogaecic and predacious lifestyle. Additionally, we identify several features that are unique to *Protanilla*.

Potential plesiomorphies of Leptanillomorpha: Our findings show that the head of Leptanillomorpha has retained few putative plesiomorphic traits. One of them is the absence of the torular apodeme. This internal process serves as area of origin for *M. tentoriohypopharyngalis* *Ohy2* in other ants (RICHTER & al. 2019, 2020) and stabilizes the antennal insertion area. It is missing in *Protanilla* and apparently also in *Opamyрма*, the presumptive sister group of the remaining Leptanillinae (WARD & FISHER 2016, YAMADA & al. 2020; Fig. 4A, B). As the torular apodeme has not been described in any other hymenopteran group, the absence is likely a retained plesiomorphy of Leptanillinae. This would also suggest that the shift of the origin of *M. tentoriohypopharyngalis* *Ohy2* to the torulus preceded the formation of the apodeme, indicating that its main function is probably related to this muscle. It cannot be ruled out that this process has been secondarily lost in the relatively small species of Leptanillinae. Simplification or reduction of endoskeletal elements is a common effect of a strongly reduced body size (e.g., POLILOV 2016, POLILOV

& al. 2019). However, with a body length of about 3 mm, *Protanilla lini* cannot be considered a miniaturized insect.

The second potentially preserved formicid ground plan feature is the origin of *M. tentorioscapalis* *lateralis* *Oan3* on the dorsal tentorial arm, which is also the case in *Leptanilla* (A. Richter, unpubl.). This character state is common in Hymenoptera (ZIMMERMANN & VILHELMSSEN 2016) and has not been found in other investigated ants so far (RICHTER & al. 2019, 2020). However, as for the previous character, this interpretation is somewhat ambiguous, as the available information on cephalic muscles of ants is still very fragmentary.

Further, we recognize three potential plesiomorphic features of Leptanillinae which are also retained in some poneroformicines, and thus likely part of the formicid ground plan. (1) A very simple external torulus, which forms a ring around the antennal insertion, is present in *Protanilla*, *Opamyрма* (YAMADA & al. 2020), and *Leptanilla* (KELLER 2011), but also occurs in several other subfamilies such as for instance Formicinae and Dorylinae (KELLER 2011). The torulus of *Martialis* has the shape of a comparatively elongate tube, but also without defined lobes (RABELING & al. 2008, BOUDINOT 2015). (2) The posterior process of the tentorium is a minute tube-like structure in the postoccipital region in *Protanilla*, the same character state as observed in *Formica rufa* LINNAEUS, 1758 (RICHTER & al. 2020), and also in other groups of Aculeata (ZIMMERMANN & VILHELMSSEN 2016). Therefore, this is very likely a ground plan feature of Formicidae, despite of frequent variations across the group (RICHTER & al. 2019, 2020). (3) The dorsal tentorial arm is confirmed as a ground plan feature of Formicidae, although it is shorter and stouter than in some of the previously described poneroformicines (RICHTER & al. 2020). See Table 2 for a general overview of head musculature in ant workers.

Leptanillomorph apomorphies: In contrast to the few retained plesiomorphic character states, we recognize that the leptanillomorph ants are highly specialized morphologically. They are characterized by a suite of apomorphies which we propose are more-or-less closely associated with the lifestyle as hypogaecic predators. For example, typical features of hypogaecic ants are reduced pigmentation, reduction of eyes, small body size, shortened appendages, and reduced or missing spinescence (WONG & GUÉNARD 2017), all of which we observe in the leptanillomorphs (BOLTON 2003, RABELING & al. 2008, YAMANE & al. 2008, BOROWIEC & al. 2011). Moreover, our results show that the protocerebral optic lobes are completely reduced in *Protanilla*. Another conspicuous feature shared by all leptanillomorphs possibly associated with the hypogaecic lifestyle is the very smooth cuticle (LOPEZ & al. 1994, BRANDÃO & al. 2010, WONG & GUÉNARD 2016, YAMADA & al. 2020), in contrast to the general condition of ants in which the cuticle has an alutaceous, imbricate, or “microreticulate” pattern that matches the boundaries of the underlying epidermal cells (CHAPMAN 2012). While cuticular surface structure is usually not phylogenetically informative on a higher taxonomic level, the consistency

of the condition observed in workers of Leptanillomorpha indicates that this could be considered as another synapomorphy of this clade. A smooth cuticle may reduce friction while moving through narrow interspaces in soil.

A synapomorphy of Formicidae is the (sub-)prognathous orientation of the head (e.g., KELLER 2011) in the females, in contrast to a clearly orthognathous head of males, a condition also found in the vast majority of other groups of Hymenoptera (e.g., BEUTEL & VILHELMSEN 2007). In the normal active posture of the ant head, the mouthparts are obliquely directed downwards (in contrast to a vertical orientation in many dead specimens). Notably different from this assumed ground plan condition in Formicidae (see, e.g., RICHTER & al. 2019, 2020), the head of leptanillomorph ants including the paired mouthparts has a horizontal orientation, similar to a truly prognathous head in other holometabolous groups like Raphidioptera or Coleoptera (BEUTEL & al. 2011). The occipital foramen is shifted posterad in leptanillomorph ants, almost opposite the mouthparts. This horizontal orientation of the head and mouthparts is likely well-suited for movements in tight spaces such as narrow tunnels and crevices in soil, similar to the strongly flattened head of geophilomorph centipedes (e.g., STOEV & al. 2015: fig. 3), the potential prey of several leptanilline species (MASUKO 1990, HSU & al. 2017, ITO & YAMANE 2020). In contrast to other prognathous insects (see above), the head of ants is not retracted into the prothorax posteriorly. The orientation of the head and mouthparts is thus highly flexible, depending on the activity. Aside from this, an orientation of the head similar to that of species of Leptanillomorpha occurs in some other groups of ants, apparently a result of convergent evolution.

An occipital carina completely enclosing the occipital region is likely linked with the unusual orientation and configuration of the head, which possibly also leads to the enlarged occipital region visible in frontal view. Both features were interpreted as potential leptanillomorph apomorphies by BOUDINOT (2015) and were statistically supported as such in ancestral state estimation (BOUDINOT & al. 2020a), albeit prone to homoplasy among ponerofomicines. However, as the occipital region is not exposed in frontal view in *Protanilla* and *Martialis* (RABELING & al. 2008), the exceptionally large size of this cephalic area might be an autapomorphy of *Opamyрма* (YAMADA & al. 2020). Another feature likely linked with advanced prognathism is the enlarged dorsal arch of the postocciput. However, the interpretation of this condition remains ambiguous as this is only documented for *Protanilla*.

Anterior shift of the antennal insertions is a state arguably linked with movements in tight spaces (LOPEZ & al. 1994, RABELING & al. 2008, YAMADA & al. 2020), and may explain the synapomorphic lack of frontal carinae (BOUDINOT & al. 2020a). As for a flattened horizontal head, this condition is also found in geophilomorphs (STOEV & al. 2015: fig. 3). A similar condition of anteriorly shifted antennal insertions also occurs in other subterranean ants such as Proceratiinae and some Dorylinae (KELLER 2011, HITA GARCIA & al. 2019). In tight subterranean spaces,

an oblique position of the antennae extending beyond the body width might restrict the movements of ants or other arthropods. Pulling the antennae back into antennal grooves – very pronounced for instance in many species of *Strumigenys* (BOLTON 1999) or *Tatuidris tatusia* BROWN & KEMPF, 1968 – could solve this problem and reduce the risk of mechanical damage for these appendages. Extending the antennae directly in front of the head is a potential alternative option, possibly enabling them to detect suitable passages through narrow interspaces. The type of antennal insertion suggests that this may apply to leptanillomorph ants. A feature linked with the antennal insertion is the almost vertically oriented mesal tentorial lamella of *Protanilla*, which results in an optimal attachment angle of the extrinsic antennal muscles. Interestingly, the mesal lamella is oriented parallel to the anterior tentorial arm in *Leptanilla* (LOPEZ & al. 1994) and in *Opamyрма* (YAMADA & al. 2020). No data on muscles of these taxa are currently available. Nevertheless, this supports the view of KELLER (2011), who emphasized the phylogenetic potential and functional importance of the antennal insertion, including its musculature and endoskeletal elements (RICHTER & al. 2020).

BOUDINOT (2015) considered “lateral mandibular bases set in deep pits” as an additional synapomorphy of Leptanillinae. The comparison of the mandibular bases of *Martialis* (BRANDÃO & al. 2010), *Opamyрма* (YAMADA & al. 2020), and *Leptanilla* (Fig. 13B) shows that the atala and ventral mandibular condyle are placed very close to each other in species of all these genera. Additionally, the atala appears to be enlarged in *Opamyрма* (YAMADA & al. 2020, fig. 2). The apparent tendency in leptanillomorphs to approximate these mandibular processes culminates in their complete fusion in *Protanilla*. Modifications of the mandibular articulation and mandibular movements, including trap-jaw mechanisms in different groups (e.g., LARABEE & SUAREZ 2014, LARABEE & al. 2017), have certainly played an important role in the evolution of ants, and should be further investigated in future studies.

An ambivalent character is the length of the scape. This segment is short in *Martialis* (RABELING & al. 2008), *Opamyрма* (YAMADA & al. 2020), and *Leptanilla* (e.g., WONG & GUÉNARD 2016, LEONG & al. 2018), whereas it is elongate and reaching the back of the head in *Protanilla*. The former condition is arguably a derived condition and part of a general trend to shortening appendages in subterranean and predacious ants, as for instance in dorylines. Even though a short scape also occurs in many stem group ants (e.g., BARDEN & GRIMALDI 2014, BORYSENKO 2017), an elongate scape as it is present in *Protanilla* and most extant groups was probably present in the last common ancestor of crown Formicidae (BARDEN 2017, BORYSENKO 2017). It appears likely that the elongation in *Protanilla* is due to reversal within the leptanillomorph clade, even though this does not conform with the general trend described above. It is conceivable that the elongated scape of *Protanilla lini* is linked with a specific trait of the life habits of the species. One possible reason is that a longer scape,

which results in a refined control of antennal movements, plays a role in the context of a trap-jaw mechanism (EHMER & GRONENBERG 1997). However, the presence of such a mandibular mechanism in *P. lini* is not fully confirmed yet. Presently, the knowledge of the biology of *Protanilla* and other leptanillines is too fragmentary for a reliable interpretation of this character.

Another ambiguous character complex is the presence of traction chaetae on the labrum and the ventral mandibular surface, with many chaetae on the mandible and only few on the labrum in the case of *Protanilla*, and the other way around in *Opomyrma* (YAMADA & al. 2020). The presence of specialized hairs on both structures was hypothesized to be another potential apomorphy of Leptanillinae by BOUDINOT (2015), even though this feature was so far not described for the genus *Leptanilla*. That mandibles with many chaetae also occur in the extinct ant genera †*Zigrasimecia* and †*Protozigrasimecia* (PERRICHOT 2014, CAO & al. 2020) shows that similar configurations have already evolved in the stem group of Formicidae. In fact, traction chaetae on the clypeus, labrum, and mandibles are common in the ant fossil record (BOUDINOT & al. 2020a). Moreover, two rows of labral traction chaetae are also present in *Apomyrma* (BROWN & al. 1970), and an array of relatively sturdy setae is also found on the ventral mandibular surface of other morphologically aberrant groups, such as the agroecomyrmecine armadillo ant *Tatuidris tatusia* (see BROWN & KEMPF 1967) or the proceratiine *Discothyrea* ROGER, 1863 (HITA GARCIA & al. 2019). The presence of specialized labral and mandibular traction chaetae is likely linked to predacious habits, as tentatively confirmed for *Tatuidris* by JACQUEMIN & al. (2014). However, the very few observations of living *Protanilla* species (e.g., HÖLLDOBLER & WILSON 1990, BILLEN & al. 2013, HSU & al. 2017) are insufficient for a reliable clarification of the function. It is apparent that similarly derived configurations have evolved several times independently. All considered, we cannot completely rule out that the expression of perioral chaetae was a feature of the formicid ground plan, with subsequent losses and secondary gains in few groups.

Autapomorphies of *Protanilla*: Beyond the remarkable structural specializations likely belonging to the ground plan of leptanillomorph ants, the species of *Protanilla* are characterized by further remarkable apomorphies. Their mandibular morphology is unique among ants in its specific configuration, and different from configurations in other trap-jaw species (see above). This complex autapomorphy involves: (1) the strong interaction of a ventral groove of the mandibular base with the hypostomal process; and (2) the rail-like guiding mechanism formed by the laterodorsal mandibular margin with the deep labral grooves. Two additional important characters are shared with the species currently assigned to the genus *Anomalomyrma* TAYLOR, 1990, indicating they are synapomorphies of Anomalomyrmini: (3) a modified dorsal mandibular articulation connected to an anterior expansion of the laterodistal clypeal region and formation

of the distoclypeal knob as supporting articulation; and (4) the fusion of the atala and the ventral condyle into a novel condylar process (BOROWIEC & al. 2011). It should however also be noted that the mandibular articulation was so far investigated in much less detail in *Anomalomyrma*, so presence of characters (1) and (2) cannot be completely ruled out in this genus. Apart from the articulation, the shape of the mandible is also unique, with its strong downward curve, the specific arrangement of small teeth with the addition of thick setae on the ventral side, and the long lateral groove. However, there is some variation in mandibular shape within the genus and Anomalomyrmini in general (BOROWIEC & al. 2011). The shape of the labrum with deep grooves and a broad, almost cup-shaped main shield should also be noted as completely unique within Formicidae described so far. Another exceptional feature is the tunnel in the mandibular base containing the mandibular gland duct opening into the mandalus. The presence of this duct is likely due to the anterior expansion of the clypeus covering the mandibular base, including the area where the mandalus is located in other ants (e.g., RICHTER & al. 2019, 2020, YAMADA & al. 2020).

An endoskeletal apomorphy of *Protanilla* is the longitudinal ridge along the midline of the clypeus. A “depressed longitudinal central furrow” of this region was described by MAN & al. (2017) for *Protanilla beijingensis*. Our data on *Protanilla lini* and reexamination of the images provided by the authors suggest that this, in fact, refers to the internal ridge visible through the partially transparent cuticle and no actual groove is present. The internal ridge likely stabilizes the extensive clypeus, which would also be an advantage in the context of a putative trap-jaw mechanism. Its formation could have also triggered the displacement of the origin of *M. clypeopalatalis* (a) *Oci1*, which is shifted to the posterior clypeal border, whereas it originates on the anterior or central clypeal region in other ants (JANET 1905, PAUL & al. 2002, RICHTER & al. 2019, 2020). With the shift of the insertion from the buccal tube to the dorsal prepharyngeal wall and its highly unusual oblique orientation when the maxillolabial complex is retracted, the entire configuration of the muscle is unique among the ants investigated so far and certainly an autapomorphy of the genus. It is currently unclear how this modification affects the function of the prepharyngeal sucking pump, but the function of this muscle is most likely to retract the anterior prepharynx when the mouthparts are retracted, rather than to play a part in the expansion of the prepharyngeal lumen to suck in fluids. Among other features such as the unusual shape of the oral arms, very long muscles *M. frontohypopharyngealis* *Ohy1* and *M. tentoriohypopharyngalis* *Ohy2*, and a very thick cuticle of the anterior prepharyngeal roof, this underlines the structural diversity of the cephalic digestive tract in ants, which was previously noted in RICHTER & al. (2020).

The inventory of glands of *Protanilla* also shows some peculiarities. The absence of the maxillary gland and presence of an internal gland in the galeolacinal complex were also observed in *Protanilla wallacei* (BILLEN & al.

2013, interpreted as stipital gland). However, due to the lack of data on glands of other leptanillomorphs and many “poneromorph” lineages, the phylogenetic interpretation remains ambiguous. As the maxillary gland is also missing in many groups outside of Formicidae (ZIMMERMANN & VILHELMSSEN 2016), it cannot be excluded that this is another plesiomorphic feature preserved in Leptanillomorpha.

Conclusion: Analyses of molecular data confirm Leptanillomorpha (Leptanillinae and *Martialis*) as the sister group of the entire remaining Formicidae. However, this does not imply that their morphology is close to the ground plan of the entire family. We identify two potentially plesiomorphic cephalic features of the leptanillomorph clade, the absence of the torular apodeme and the origin of an extrinsic antennal muscle on the dorsal tentorial arm. An entire series of morphological features reveals the Leptanillomorpha as a group of highly specialized subterranean and predacious ants, among them the reduction of eyes and associated brain regions, a posteriorly shifted occipital foramen resulting in a pronouncedly prognathous head associated with a completely closed occipital carina, an anterior shift of the antennal insertions, the absence of the frontal carinae, and modifications of the mandibular articulation.

The features described above and conditions found in stem group ants (BOUDINOT & al. 2020) cast some doubt on a hypogaecic origin of Formicidae, as suggested by recent analyses of molecular data (LUCKY & al. 2013, NELSON & al. 2018). This would imply some unlikely reversals, as for instance the secondary gain of functional eyes and optic neuropils. *Protanilla* is highly specialized, with a unique mechanism of mandibular movements associated with complex modifications of the shape and articulation of the mandibles, and also conspicuous deep lateral grooves of the labrum. Additional potential apomorphies of *Protanilla* include features of the endoskeleton, cephalic digestive tract, and glandular system. Our results add relevant information for reconstructing the cephalic ground plan of ants and character transformations in the evolution of the group. They also draw attention to a highly unusual mandibular articulation and mechanisms of *Protanilla*. High-speed observations of living individuals could help to confirm (or refute) a power-amplification mechanism in future studies.

Acknowledgments

We thank the OIST Imaging Section for providing access to the μ -CT scanner, especially Shinya Komoto for his helpful supervision, and the OIST Scientific Computing & Data Analysis Section, especially Pavel Puchenkov, for providing a script to infer rotational movement in Blender. We are very grateful to Chung-Chi Lin and Mark K. L. Wong for collecting and providing specimens used in this study, and to Mark K. L. Wong for providing links to his informative YouTube videos of living *Protanilla* and allowing us to download one of them to include in the supplementary material, to An Vandoren for making

the serial histological sections, and to Kenny Jandausch for assistance in video-recording experiments with a 3D printed *Protanilla lini* head. We further extend our gratitude to the two anonymous reviewers and the editorial team of Myrmecological News who helped to greatly improve this manuscript through their excellent criticism and suggestions. This work was partly funded by subsidy funding to OIST. BEB acknowledges support from the Alexander von Humboldt Stiftung. A scholarship of the Evangelisches Studienwerk Villigst e.V. to Adrian Richter is also gratefully acknowledged.

References

- AGOSTI, D., MAJER, J., ALONSO, E. & SCHULTZ, T.R. 2000: Ants: standard methods for measuring and monitoring biodiversity. – Smithsonian Institution Press, Washington, DC, XXI + 280 pp.
- BAIDYA, P. & BAGCHI, S. 2020: A new species of *Protanilla* TAYLOR 1990 (Hymenoptera: Formicidae: Leptanillinae) from India. – *Halteres* 11: 19-24.
- BARDEN, P. 2017: Fossil ants (Hymenoptera: Formicidae): ancient diversity and the rise of modern lineages. – *Myrmecological News* 24: 1-30.
- BARDEN, P. & GRIMALDI, D. 2013: A new genus of highly specialized ants in Cretaceous Burmese amber (Hymenoptera: Formicidae). – *Zootaxa* 3681: 405-412.
- BARDEN, P. & GRIMALDI, D. 2014: A diverse ant fauna from the mid-Cretaceous of Myanmar (Hymenoptera: Formicidae). – *Public Library of Science One* 9: art. e93627.
- BARONI URBANI, C. 1977: Materiali per una revisione della sottofamiglia Leptanillinae EMERY (Hymenoptera: Formicidae). – *Entomologica Brasiliensia* 2: 427-488.
- BARONI URBANI, C., BOLTON, B. & WARD, P.S. 1992: The internal phylogeny of ants (Hymenoptera: Formicidae). – *Systematic Entomology* 17: 301-329.
- BARONI URBANI, C. & DE ANDRADE, M. 2007: The ant tribe Dacetini: limits and constituent genera, with descriptions of new species. – *Annali del Museo Civico di Storia Naturale Giacomo Doria (Genova)* 99: 1-191.
- BEUTEL, R.G., FRIEDRICH, F., HÖRNSCHEMEYER, T., POHL, H., HÜNEFELD, F., BECKMANN, F., MEIER, R., MISOF, B., WHITING, M.F. & VILHELMSSEN, L. 2011: Morphological and molecular evidence converge upon a robust phylogeny of the megadiverse Holometabola. – *Cladistics* 27: 341-355.
- BEUTEL, R.G., FRIEDRICH, F., YANG, X.-K. & GE, S.-Q. 2014: Insect morphology and phylogeny: a textbook for students of entomology. – Walter de Gruyter, Berlin, 532 pp.
- BEUTEL, R.G. & VILHELMSSEN, L. 2007: Head anatomy of Xyelidae (Hexapoda: Hymenoptera) and phylogenetic implications. – *Organisms Diversity & Evolution* 7: 207-230.
- BHARTI, H. & AKBAR, S.A. 2015: First record of genus *Protanilla* (Hymenoptera: Formicidae: Leptanillinae) from India with description of a new species. – *Journal of Asia-Pacific Entomology* 18: 573-576.
- BILLEN, J., BAUWELEERS, E., HASHIM, R. & ITO, F. 2013: Survey of the exocrine system in *Protanilla wallacei* (Hymenoptera, Formicidae). – *Arthropod Structure & Development* 42: 173-183.
- BILLEN, J., ITO, F., MAILE, R. & MORGAN, E.D. 1998: The mandibular gland, probably the source of the alarm substance in *Leptanilla* sp. (Hymenoptera, Formicidae). – *Naturwissenschaften* 85: 596-597.

- BLANKE, A. 2019: The early evolution of biting-chewing performance in Hexapoda. In: KRENN, H.W. (Ed.): *Insect mouthparts*. – Springer, Cham, pp. 175-202.
- BOLTON, B. 1990: The higher classification of the ant subfamily Leptanillinae (Hymenoptera: Formicidae). – *Systematic Entomology* 15: 267-282.
- BOLTON, B. 1999: Ant genera of the tribe Dacetoniini (Hymenoptera: Formicidae). – *Journal of Natural History* 33: 1639-1689.
- BOLTON, B. 2003: Synopsis and classification of Formicidae. – *Memoirs of the American Entomological Institute* 71: 1-370.
- BOLTON, B. 2020: An online catalog of the ants of the world. – <<https://antcat.org>>, retrieved on 14 September 2020.
- BOLTON, B. & FISHER, B.L. 2008: Afrotropical ants of the ponerine genera *Centromyrmex* MAYR, *Promyopias* SANTSCHI gen. rev. and *Feroponera* gen. n., with a revised key to genera of African Ponerinae (Hymenoptera: Formicidae). – *Zootaxa* 1929: 1-37.
- BOOHER, D.B., GIBSON, J.C., LIU, C., LONGINO, J.T., FISHER, B.L., JANDA, M., NARULA, N., TOULKERIDOU, E., MIKHEYEV, A.S. & SUAREZ, A.V. 2021: Functional innovation promotes diversification of form in the evolution of an ultrafast trap-jaw mechanism in ants. – *Public Library of Science Biology* 19: art. e3001031.
- BOROWIEC, M.L., RABELING, C., BRADY, S.G., FISHER, B.L., SCHULTZ, T.R. & WARD, P.S. 2019: Compositional heterogeneity and outgroup choice influence the internal phylogeny of the ants. – *Molecular phylogenetics and evolution* 134: 111-121.
- BOROWIEC, M.L., SCHULZ, A., ALPERT, G.D. & BAÑAR, P. 2011: Discovery of the worker caste and descriptions of two new species of *Anomalomyrma* (Hymenoptera: Formicidae: Leptanillinae) with unique abdominal morphology. – *Zootaxa* 2810: 1-14.
- BORYSENKO, L.H. 2017: Description of a new genus of primitive ants from Canadian amber, with the study of relationships between crown ants and stem ants (Hymenoptera: Formicidae). – *Insecta Mundi* 570: 1-57.
- BOUDINOT, B.E. 2015: Contributions to the knowledge of Formicidae (Hymenoptera, Aculeata): a new diagnosis of the family, the first global male-based key to subfamilies, and a treatment of early branching lineages. – *European Journal of Taxonomy* 120: 1-62.
- BOUDINOT, B.E., KHOURI, Z., RICHTER, A., VAN DE KAMP, T., BARDEN, P., PERRICHOT, V. & CHAUL, J.C.M. 2020a: Chapter II. The evolution of the ants: Extinct ant sister-group illuminates eusociality origin and post-K/Pg persistence. Pp. 174-393. In: BOUDINOT, B.E. 2020: *Systematic and evolutionary morphology; Case studies on Formicidae, Mesozoic Aculeata and Hexapodan genitalia*. – University of California, Davis, CA, 562 pp.
- BOUDINOT, B.E., PERRICHOT, V. & CHAUL, J.C.M. 2020b: †*Camelosphecia* gen. nov., lost ant-wasp intermediates from the mid Cretaceous (Hymenoptera, Formicoidea). – *ZooKeys* 1005: 21-55.
- BRADY, S.G., SCHULTZ, T.R., FISHER, B.L. & WARD, P.S. 2006: Evaluating alternative hypotheses for the early evolution and diversification of ants. – *Proceedings of the National Academy of Sciences of the United States of America* 103: 18172-18177.
- BRADY, S.G. & WARD, P.S. 2005: Morphological phylogeny of army ants and other dorylomorphs (Hymenoptera: Formicidae). – *Systematic Entomology* 30: 593-618.
- BRANDÃO, C.R.F., DINIZ, J.L.M. & FEITOSA, R.M. 2010: The venom apparatus and other morphological characters of the ant *Martialis heureka* (Hymenoptera, Formicidae, Martialinae). – *Papéis Avulsos de Zoologia (São Paulo)* 50: 413-423.
- BRANSTETTER, M.G., LONGINO, J.T., WARD, P.S. & FAIRCLOTH, B.C. 2017: Enriching the ant tree of life: enhanced UCE bait set for genome-scale phylogenetics of ants and other Hymenoptera. – *Methods in Ecology and Evolution* 8: 768-776.
- BROWN, W.L. 1953: Revisionary studies in the ant tribe Dacetini. – *The American Midland Naturalist* 50: 1-137.
- BROWN, W.L. & KEMPF, W.W. 1967: *Tatuidris*, a remarkable new genus of Formicidae (Hymenoptera). – *Psyche* 74: 183-190.
- BROWN, W.L., LEVIEUX, J. & GOTWALD JR., W.H. 1970: A new genus of ponerine ants from West Africa. – *Psyche* 77: 259-275.
- CAO, H., BOUDINOT, B.E., WANG, Z., MIAO, X., SHIH, C., REN, D. & GAO, T. 2020: Two new iron maiden ants from Burmese amber (Hymenoptera: Formicidae: †Zigrasimeciini). – *Myrmecological News* 30: 161-173.
- CHAPMAN, R.F., SIMPSON, S.J. & DOUGLAS, A.E. (Eds.) 2012: *The insects: structure and function*, 5th edn. – Cambridge University Press, Cambridge, UK, 929 pp.
- DUNCAN, C.D. 1969: A contribution to the biology of North American vespine wasps. – *Stanford University Publications, Biological Sciences* 8: 1-272.
- EHMER, B. & GRONENBERG, W. 1997: Antennal muscles and fast antennal movements in ants. – *Journal of Comparative Physiology B* 167: 287-296.
- EMERY, C. 1904: Le affinità del genere *Leptanilla* e i limiti delle Dorylinae. – *Archivio Zoologico* 2: 107-116.
- ENGELKES, K., FRIEDRICH, F., HAMMEL, J.U. & HAAS, A. 2018: A simple setup for episcopic microtomy and a digital image processing workflow to acquire high-quality volume data and 3D surface models of small vertebrates. – *Zoomorphology* 137: 213-228.
- FISHER, B.L. 1999: Improving inventory efficiency: a case study of leaf-litter ant diversity in Madagascar. – *Ecological Applications* 9: 714-731.
- GOTWALD, W.H. 1969: Comparative morphological studies of the ants: with particular reference to the mouthparts (Hymenoptera: Formicidae). – *New York State College of Agriculture, Ithaca, NY*, 150 pp.
- GRIEBENOW, Z.H. 2020a: Synonymization of the male-based ant genus *Phaulomyrma* (Hymenoptera, Formicidae) with *Leptanilla* based upon Bayesian total-evidence phylogenetic inference. – bioRxiv; doi: 10.1101/2020.08.28.272799.
- GRIEBENOW, Z.H. 2020b: Delimitation of tribes in the subfamily Leptanillinae (Hymenoptera: Formicidae), with a description of the male of *Protanilla lini* TERAYAMA, 2009. – *Myrmecological News* 30: 229-250.
- GRONENBERG, W. 1995: The fast mandible strike in the trap-jaw ant *Odontomachus*. – *Journal of Comparative Physiology A: Neuroethology, Sensory, Neural, and Behavioral Physiology* 176: 391-398.
- GRONENBERG, W. 1996: The trap-jaw mechanism in the dacetine ants *Daceton armigerum* and *Strumigenys* sp. – *Journal of Experimental Biology* 199: 2021-2033.
- GRONENBERG, W., BRANDÃO, C.R.F., DIETZ, B.H. & JUST, S. 1998: Trap-jaws revisited: the mandible mechanism of the ant *Acanthognathus*. – *Physiological Entomology* 23: 227-240.
- GRONENBERG, W., PAUL, J., JUST, S. & HÖLLDOBLER, B. 1997: Mandible muscle fibers in ants: fast or powerful? – *Cell and Tissue Research* 289: 347-361.
- HITA-GARCIA, F., LIEBERMAN, Z., AUDISIO, T.L., LIU, C. & ECONOMO, E.P. 2019: Revision of the highly specialized ant genus *Discothyrea* (Hymenoptera: Formicidae) in the Afrotropics with X-ray microtomography and 3D cybertaxonomy. – *Insect Systematics and Diversity* 3: art. 5.

- HÖLLDOBLER, B. & WILSON, E.O. 1990: The ants. – Harvard University Press, Cambridge, MA, 732 pp.
- HSU, P.-W., HSU, F.-C., HSIAO, Y. & LIN, C.-C. 2017: Taxonomic notes on the genus *Protanilla* (Hymenoptera: Formicidae: Leptanillinae) from Taiwan. – *Zootaxa* 4268: 117-130.
- ITO, F. & YAMANE, S. 2020: Behavior of the queen of *Leptanilla clypeata* YAMANE et Ito collected in the Bogor Botanical Gardens, West Java, Indonesia (Hymenoptera; Formicidae), with a note on colony composition and a description of the ergatoid queen. – *Asian Myrmecology* 12: art. e012004.
- JACQUEMIN, J., DELSINNE, T., MARAUN, M. & LEPONCE, M. 2014: Trophic ecology of the armadillo ant, *Tatuidris tatusia*, assessed by stable isotopes and behavioral observations. – *Journal of Insect Science* 14: art. 108.
- JANET, C. 1905: Anatomie de la tête du *Lasius niger*. Reine. – Limoges Imprimerie-Librairie Ducourtieux et Gout, Limoges, 40 pp.
- KELLER, R.A. 2011: A phylogenetic analysis of ant morphology (Hymenoptera: Formicidae) with special reference to the poneromorph subfamilies. – *Bulletin of the American Museum of Natural History* 355: 1-90.
- KELLER, R.A. & PEETERS, C. 2020: Poneroid ants. In: STARR, C. (Ed.): *Encyclopedia of social insects*. – Springer International Publishing, Cham, pp. 1-6.
- KRONAUER, D.J.C. 2009: Recent advances in army ant biology (Hymenoptera: Formicidae). – *Myrmecological News* 12: 51-65.
- KUGLER, C. 1992: Stings of ants of the Leptanillinae (Hymenoptera: Formicidae). – *Psyche* 99: 103-115.
- KUGLER, J. 1987: The Leptanillinae (Hymenoptera: Formicidae). – *Israel Journal of Entomology* 20: 45-57.
- KÜCK, P., GARCIA, F.H., MISOF, B. & MEUSEMANN, K. 2011: Improved phylogenetic analyses corroborate a plausible position of *Martialis heureka* in the ant tree of life. – *Public Library of Science One* 6: art. e21031.
- LARABEE, F.J., GRONENBERG, W. & SUAREZ, A.V. 2017: Performance, morphology and control of power-amplified mandibles in the trap-jaw ant *Myrmoteras* (Hymenoptera: Formicidae). – *Journal of Experimental Biology* 220: 3062-3071.
- LARABEE, F.J. & SUAREZ, A.V. 2014: The evolution and functional morphology of trap-jaw ants (Hymenoptera: Formicidae). – *Myrmecological News* 20: 25-36.
- LEONG, C.-M., YAMANE, S. & GUÉNARD, B. 2018: Lost in the city: discovery of the rare ant genus *Leptanilla* (Hymenoptera: Formicidae) in Macau with description of *Leptanilla macauensis* sp. nov. – *Asian Myrmecology* 10: art. e010001.
- LÓPEZ, F., MARTÍNEZ, M. & BARANDICA, J. 1994: Four new species of the genus *Leptanilla* (Hymenoptera: Formicidae) from Spain – relationships to other species and ecological issues. – *Sociobiology* 24: 179-212.
- LÖSEL, P. & HEUVELINE, V. 2016: Enhancing a diffusion algorithm for 4D image segmentation using local information. – *SPIE Medical Imaging* 9784: art. 97842L.
- LÖSEL, P.D., VAN DE KAMP, T., JAYME, A., ERSHOV, A., FARAGÓ, T., PICHLER, O., JEROME, N.T., AADEPU, N., BREMER, S., CHILINGARYAN, S.A., HEETHOFF, M., KOPMANN, A., ODAR, J., SCHMELZLE, S., ZUBER, M., WITTBRODT, J., BAUMBACH, T. & HAUVELINE, V. 2020: Introducing Biomedisa as an open-source online platform for biomedical image segmentation. – *Nature Communications* 11: art. 5577.
- LUCKY, A., TRAUTWEIN, M.D., GUÉNARD, B.S., WEISER, M.D. & DUNN, R.R. 2013: Tracing the rise of ants-out of the ground. – *Public Library of Science One* 8: art. e84012.
- MAN, P., RAN, H., CHEN, Z. & XU, Z. 2017: The northern-most record of Leptanillinae in China with description of *Protanilla beijingensis* sp. nov. (Hymenoptera: Formicidae). – *Asian Myrmecology* 9: 1-12.
- MASUKO, K. 1989: Larval hemolymph feeding in the ant *Leptanilla japonica* by use of a specialized duct organ, the “larval hemolymph tap” (Hymenoptera: Formicidae). – *Behavioral Ecology and Sociobiology* 24: 127-132.
- MASUKO, K. 1990: Behavior and ecology of the enigmatic ant *Leptanilla japonica* BARONI URBANI (Hymenoptera: Formicidae: Leptanillinae). – *Insectes Sociaux* 37: 31-57.
- MICHENER, C.D. & FRASER, A. 1978: A comparative anatomical study of mandibular structure in bees (Hymenoptera: Apoidea). – *University of Kansas Science Bulletin* 51: 463-482.
- MOREAU, C.S. & BELL, C.D. 2013: Testing the museum versus cradle tropical biological diversity hypothesis: phylogeny, diversification, and ancestral biogeographic range evolution of the ants. – *Evolution* 67: 2240-2257.
- MOREAU, C.S., BELL, C.D., VILA, R., ARCHIBALD, S.B. & PIERCE, N.E. 2006: Phylogeny of the ants: diversification in the age of angiosperms. – *Science* 312: 101-104.
- NELSEN, M.P., REE, R.H. & MOREAU, C.S. 2018: Ant-plant interactions evolved through increasing interdependence. – *Proceedings of the National Academy of Sciences of the United States of America* 115: 12253-12258.
- OGATA, K., TERAYAMA, M. & MASUKO, K. 1995: The ant genus *Leptanilla*: discovery of the worker-associated male of *L. japonica*, and a description of a new species from Taiwan (Hymenoptera: Formicidae: Leptanillinae). – *Systematic Entomology* 20: 27-34.
- PATEK, S., BAIO, J., FISHER, B. & SUAREZ, A. 2006: Multifunctionality and mechanical origins: ballistic jaw propulsion in trap-jaw ants. – *Proceedings of the National Academy of Sciences of the United States of America* 103: 12787-12792.
- PAUL, J. & GRONENBERG, W. 1999: Optimizing force and velocity: mandible muscle fibre attachments in ants. – *Journal of Experimental Biology* 202: 797-808.
- PAUL, J., ROCES, F. & HÖLLDOBLER, B. 2002: How do ants stick out their tongues? – *Journal of Morphology* 254: 39-52.
- PERRAULT, G.H. 1999: Étude morphoanatomique et biométrique du métasoma antérieur des ouvrières. Contribution à la systématique et à la phylogénie des fourmis (Hymenoptera: Formicidae). – *Annales de la Société entomologique de France* 40: 291-371.
- PERRICHOT, V. 2014: A new species of the Cretaceous ant *Zigrasimecia* based on the worker caste reveals placement of the genus in the Sphecomyrminae (Hymenoptera: Formicidae). – *Myrmecological News* 19: 165-169.
- PETERSEN, B. 1968: Some novelties in presumed males of Leptanillinae (Hym., Formicidae). – *Entomologiske Meddelelser* 36: 577-598.
- POHL, H. 2010: A scanning electron microscopy specimen holder for viewing different angles of a single specimen. – *Microscopy Research and Technique* 73: 1073-1076.
- POLILOV, A.A. 2016: At the size limit-effects of miniaturization in insects. – Springer International Publishing, Cham, 335 pp.
- POLILOV, A.A., RIBERA, I., YAVORSKAYA, M.I., CARDOSO, A., GREBENNIKOV, V.V. & BEUTEL, R.G. 2019: The phylogeny of Ptiliidae (Coleoptera: Staphylinoidea) – the smallest beetles and their evolutionary transformations. – *Arthropod Systematics & Phylogeny* 77: 433-455.
- RABELING, C., BROWN, J.M. & VERHAAGH, M. 2008: Newly discovered sister lineage sheds light on early ant evolution. – *Proceedings of the National Academy of Sciences of the United States of America* 105: 14913-14917.

- RICHTER, A., GARCIA, F.H., KELLER, R.A., BILLEN, J., ECONOMO, E.P. & BEUTEL, R.G. 2020: Comparative analysis of worker head anatomy of *Formica* and *Brachyponera* (Hymenoptera: Formicidae). – *Arthropod Systematics & Phylogeny* 78: 133-170.
- RICHTER, A., KELLER, R.A., ROSUMEK, F.B., ECONOMO, E.P., HITA GARCIA, F. & BEUTEL, R.G. 2019: The cephalic anatomy of workers of the ant species *Wasmannia affinis* (Formicidae, Hymenoptera, Insecta) and its evolutionary implications. – *Arthropod Structure & Development* 49: 26-49.
- SCHINDELIN, J., ARGANDA-CARRERAS, I., FRISE, E., KAYNIG, V., LONGAIR, M., PIETZSCH, T., PREIBISCH, S., RUEDEN, C., SAALFELD, S., SCHMID, B., TINEVEZ, J.-Y., WHITE, D.J., HARTENSTEIN, V., ELICEIRI, K., TOMANCAK, P. & CARDONA, A. 2012: Fiji: an open-source platform for biological-image analysis. – *Nature Methods* 9: 676-682.
- SCHMIDT, F. & SOLAR, R. 2010: Hypogaecic pitfall traps: methodological advances and remarks to improve the sampling of a hidden ant fauna. – *Insectes Sociaux* 57: 261-266.
- STOEV, P., AKKARI, N., KOMERIČKI, A., EDGECOMBE, G.D. & BONATO, L. 2015: At the end of the rope: *Geophilus hadesi* sp. n. – the world's deepest cave-dwelling centipede (Chilopoda, Geophilomorpha, Geophilidae). – *ZooKeys* 510: 95-114.
- WANG, Z., ZHANG, W., WU, J. & YANG, Y. 2020: An approach to observing and quantifying real-time mandibular muscle topology in the trap-jaw ant *Odontomachus monticola* by synchrotron imaging. – *Journal of Insect Behavior* 33: 174-183.
- WARD, P.S. 2014: The phylogeny and evolution of ants. – *Annual Review of Ecology, Evolution, and Systematics* 45: 23-43.
- WARD, P.S. & FISHER, B.L. 2016: Tales of dracula ants: the evolutionary history of the ant subfamily Amblyoponinae (Hymenoptera: Formicidae). – *Systematic Entomology* 41: 683-693.
- WHEELER, G.C. & WHEELER, E.W. 1930: Two new ants from Java. – *Psyche* 37: 193-201.
- WILKIE, K.T.R., MERTL, A.L. & TRANIELLO, J.F.A. 2007: Biodiversity below ground: probing the subterranean ant fauna of Amazonia. – *Naturwissenschaften* 94: 725-731.
- WILSON, E.O. 1955: A monographic revision of the ant genus *Lasius*. – *Bulletin of the Museum of Comparative Zoology* 113: 1-199.
- WIPFLER, B., MACHIDA, R., MÜLLER, B. & BEUTEL, R.G. 2011: On the head morphology of Grylloblattodea (Insecta) and the systematic position of the order, with a new nomenclature for the head muscles of Dicondylia. – *Systematic Entomology* 36: 241-266.
- WONG, M.K.L. & GUÉNARD, B. 2016: *Leptanilla hypodracos* sp. n., a new species of the cryptic ant genus *Leptanilla* (Hymenoptera, Formicidae) from Singapore, with new distribution data and an updated key to Oriental *Leptanilla* species. – *ZooKeys* 551: 129-144.
- WONG, M. & GUÉNARD, B. 2017: Subterranean ants: summary and perspectives on field sampling methods, with notes on diversity and ecology (Hymenoptera: Formicidae). – *Myrmecological News* 25: 1-16.
- WONG, M.K.L. & GUÉNARD, B. 2020: Subterranean ants. In: STARR, C. (Ed.): *Encyclopedia of social insects*. – Springer International Publishing, Cham, pp. 1-6.
- XU, Z.-H. 2012: *Furcotanilla*, a new genus of the ant subfamily Leptanillinae from China with descriptions of two new species of *Protanilla* and *P. rafflesi* Taylor (Hymenoptera: Formicidae). – *Sociobiology* 59: 477-491.
- YAMADA, A., NGUYEN, D.D. & EGUCHI, K. 2020: Unveiling the morphology of the oriental rare monotypic ant genus *Opamyрма* Yamane, Bui & Eguchi, 2008 (Hymenoptera: Formicidae: Leptanillinae) and its evolutionary implications, with first descriptions of the male, larva, tentorium, and sting apparatus. – *Myrmecological News* 30: 27-52.
- YAMANE, S., BUI, T.V. & EGUCHI, K. 2008: *Opamyрма hungvuong*, a new genus and species of ant related to *Apomyрма* (Hymenoptera: Formicidae: Amblyoponinae). – *Zootaxa* 1767: 55-63.
- ZHANG, W., LI, M., ZHENG, G., GUAN, Z., WU, J. & WU, Z. 2020: Multifunctional mandibles of ants: variation in gripping behavior facilitated by specific microstructures and kinematics. – *Journal of Insect Physiology* 120: art. 103993.
- ZIMMERMANN, D. & VILHELMSSEN, L. 2016: The sister group of Aculeata (Hymenoptera) – evidence from internal head anatomy, with emphasis on the tentorium. – *Arthropod Systematics & Phylogeny* 74: 195-218.